Cardiovascular Diabetology

RESEARCH

Open Access

Endothelial cells derived extracellular vesicles promote diabetic arterial calcification via circ_0008362/miR-1251-5p/Runx2 axial

Xiao Lin[1†], Sha-Qi He[1†], Su-Kang Shan[2], Feng Xu[2], Feng Wu[3], Fu-Xing-Zi Li[2], Ming-Hui Zheng[2], Li-Min Lei[2], Jia-Yue Duan[2], Yun-Yun Wu[2], Yan-Lin Wu[2], Ke-Xin Tang[2], Rong-Rong Cui[2], Bei Huang[1], Jun-Jie Yang[4], Xiao-Bo Liao[5], Jun Liu[1,6*] and Ling-Qing Yuan[2*]

Abstract

Introduction Arterial calcification, an independent predictor of cardiovascular events, increases morbidity and mortality in patients with diabetes mellitus (DM), but its mechanisms remain unclear. Extracellular vesicles (EVs) play an important role in intercellular communication. The study investigates the role and potential mechanisms of EVs derived from endothelial cells (ECs) in regulating vascular smooth muscle cell (VSMC) calcification under high glucose (HG) condition, with a goal of developing effective prevention and treatment strategies for diabetic arterial calcification.

Results The results showed that EVs derived from HG induced ECs (EC^{HG}-EVs) exhibited a bilayer structure morphology with a mean diameter of 74.08 ± 31.78 nm, expressing EVs markers including CD9, CD63 and TSG101, but not express calnexin. EC^{HG}-EVs was internalized by VSMCs and induced VSMC calcification by increasing Runx2 expression and mineralized nodule formation. The circ_0008362 was enriched in EC^{HG}-EVs, and it can be transmitted to VSMCs to promote VSMC calcification both in vitro and in vivo. Mechanistically, miR-1251-5p might be one of the targets of circ_0008362 and they were co-localization in the cytoplasm of VSMCs. Runx2 was identified as the downstream target of miR-1251-5p, and circ_0008362 acted as a sponge, enhancing Runx2 expression and then promoted VSMC calcification. Besides, circ_0008362 could directly interact with Runx2 to aggravate VSMC calcification. Notably, DiR-labelled EC^{HG}-EVs was detected in the vessels of mice. Meanwhile, the level of circ_0008362 and Runx2 were increased significantly, while the expression of miR-1251-5p was decreased significantly in calcified artery tissues of mice. However, inhibiting the release of EVs by GW4869 attenuated arterial calcification in diabetic mice. Finally, the level of circulation of plasma EVs circ_0008362 was significantly higher in patients with DM compared with normal controls. Elevated levels of plasma EVs circ_0008362 were associated with more severe coronary and aorta artery calcification in patients with DM.

†Xiao Lin and Sha-Qi He have equally contributed to this work.

*Correspondence:
Jun Liu
junliu123@csu.edu.cn
Ling-Qing Yuan
allenylq@csu.edu.cn

Full list of author information is available at the end of the article

Conclusions Our findings suggested that circ_0008362 was enriched in EVs derived from ECs and promoted VSMC calcification under HG conditions, both by sponging miR-1251-5p to upregulate Runx2 expression and through direct interaction with Runx2. Furthermore, elevated levels of plasma EVs circ_0008362 were associated with more severe coronary and aorta artery calcification in patients with DM. These results may serve as a potential prevention and therapeutic target for diabetic arterial calcification.

Graphical abstract

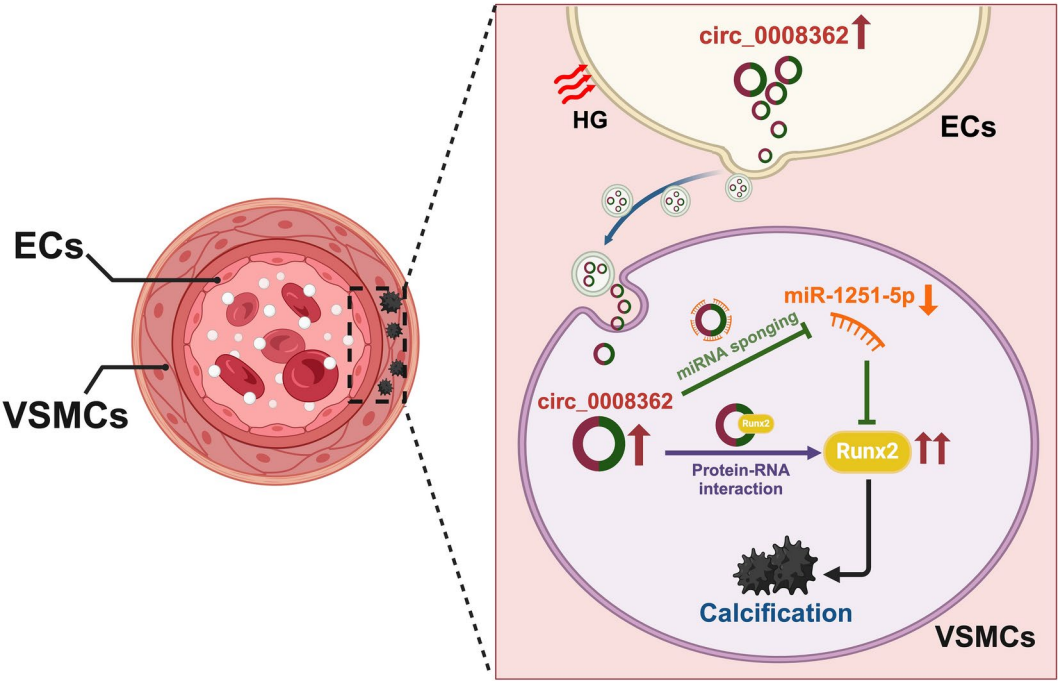

Keywords Extracellular vesicles, Circ_0008362, Endothelial cells, Vascular smooth muscle cells, Arterial calcification, Diabetes mellitus

Introduction

Arterial calcification is mainly characterized as the pathological deposition of mineral in the vessel wall, especially medial calcification (also known as Mönckeberg's calcification) [1, 2]. It is an independent predictor of cardiovascular events and increase morbidity and mortality of cardiovascular diseases, particularly in patients with diabetes mellitus (DM) [3, 4]. Studies have demonstrated that the trans-differentiation of vascular smooth muscle cells (VSMCs) into osteoblast-like cells is the pivotal pathological factor in arterial calcification [2, 5]. In patients with DM, high glucose (HG) has been considered to be the main cause of arterial calcification [6]. However, prevention and treatment of diabetic arterial calcification is not just as simple as lowering blood glucose. The ADVANCE study showed that long-term intensive glucose control had no significant macrovascular benefits, and failed to reduce the incidence of macrovascular events and all-cause mortality [7]. Therefore, the precise molecular mechanism of arterial calcification in patients with DM remains incompletely understood and that needs further study.

Endothelial cells (ECs) and VSMCs are the two main cells maintaining the vascular structure and function. ECs are located in the inner layer of blood vessel walls, which are directly stimulated by various components in the blood, such as hyperglycemia, and resulting in atherosclerosis and calcification [5, 8]. However, arterial calcification mainly occurs in the media layer of blood vessel walls in patients with DM, which characterized by VSMC calcification [4, 6]. Although studies had demonstrated that there existed intercellular communication between ECs and VSMCs via direct contact or paracrine signaling [2]. The detailed mechanism by which ECs affect the functions of VSMCs remains unknown.

Extracellular vesicles (EVs) are small (average diameter of 40–200 nm) membrane-derived structures released into the extracellular space by various cell types [9]. Recent studies have demonstrated that EVs-based carriers have been identified as efficient vehicles

for transferring proteins, RNAs, and lipids between cells, delivering their contents to target cells [9, 10]. For example, miR-483-5p and miR-2861 were enriched in aged bone matrix derived-EVs and exacerbated vascular calcification [11]. Our previous study also demonstrated that EVs derived from melatonin-treated VSMCs could mitigate arterial calcification and aging through the paracrine action of miR-204/miR-211 [12]. Recently, our team found that adventitial fibroblasts derived EVs promoted VSMC calcification by delivering miR-21-5p under high phosphorus condition [13]. However, the potential role of EVs in mediating intercellular communication between ECs and VSMCs under hyperglycemia remains unclear.

Circular RNAs (circRNAs), regarded as a novel regulator in human diseases, constitute a large class of non-coding RNAs (ncRNAs) that arise from the back-splicing of pre-messenger RNAs (pre-mRNA) [14]. Numerous circRNAs have been implicated in a variety of human diseases, including but not limited to diabetes, neurological disorders, cardiovascular diseases, and malignancies [15]. Recent studies have revealed that circRNAs possess multifaceted functions, including acting as microRNA (miRNA) sponges, binding partners of proteins, and regulators of gene expression. Additionally, they can also undergo translation to participate in protein synthesis [14, 16]. For instance, circRNA_0077930 had been reported to be abundant and stable in the exosome-derived from HG-induced ECs, and then regulated VSMC senescence [16]. However, the comprehensive pathophysiological functions of circRNAs in regulating arterial calcification remain largely elusive.

In the present study, we investigate the crosstalk between ECs and VSMCs, with a focus on elucidating the mechanisms of hsa_circ_0008362 in EVs derived from ECs involving in modulating VSMC calcification under hyperglycemia. Firstly, we have discovered that EVs-derived from HG induced ECs (EC^{HG}-EVs) can be taken up by VSMCs and have the ability to regulate VSMC calcification both in vitro and in vivo. Then, EC^{HG}-EVs transport hsa_circ_0008362 to VSMCs and promote VSMC calcification through two pathways: hsa_circ_0008362, on the one hand, would sponge with miR-1251-5p to upregulate its target gene Runt-related transcription factor 2 (Runx2) expression. On the other hand, hsa_circ_0008362 could directly regulate Runx2 expression by binding to Runx2 protein. Finally, we find that the increased level of plasma EVs hsa_circ_0008362 is associated with artery calcification in patients with DM. Taken together, our current study reveals the key role of hsa_circ_0008362 in regulating diabetic arterial calcification and provide a potential target and direction for predicting and treating arterial calcification in patients with DM.

Results

EC^{HG}-EVs could be taken up by VSMCs and promote VSMC calcification

In order to explore the role of EC^{HG}-EVs in regulating VSMC calcification, we extracted the EVs derived from ECs using ultracentrifugation. As previous reported [2], the isolated EVs displayed cup-shaped morphologies with a mean diameter of 74.08 ± 31.78 nm, as revealed by transmission electron microscopy (TEM; Fig. 1A) and nanoparticle tracking analysis (NTA; Fig. 1B). Western blot (WB) analysis further confirmed the isolated EVs exhibited classical EV markers CD9, CD63, and TSG101, but no negative marker Calnexin. Besides, there also existed EC-specific markers CD31 and CD144, but without the foetal bovine serum (FBS) marker bovine serum albumin (BSA) (Fig. 1C; supplemental Fig. 1A). These data verified that the isolated EVs were indeed derived from ECs without contaminated by FBS-derived EVs, which indicating the purity and characteristics of EVs. Moreover, the concentration of EC^{HG}-EVs was significantly increased compared to that derived from normal-glucose induced ECs (EC^{NG}-EVs) (supplemental Fig. 1B).

Next, laser confocal scanning electron microscopy and Z-stack analysis revealed that PKH26-labelled EC-EVs could be taken up by VSMCs and mainly located at the cytoplasm of VSMCs (Fig. 1D, E). Furthermore, alizarin red s staining (ARS) revealed a significant increase in mineralized nodules formation in VSMCs induced by EC^{HG}-EVs for 14 days (Fig. 1F). Additionally, the level of Runx2 and BMP2 protein, as well as ALP positive staining area was significantly increased in VSMCs treated with EC^{HG}-EVs compared to other groups (Fig. 1G; supplemental Fig. 1C, D). However, the supernatant derived from HG induced ECs with deprivation of EVs (EC^{HG}-Sup^{-EVs}) seems had no significant effect on VSMC calcification (Fig. 1F, G; supplemental Fig. 1C, D). Besides, the trans-well co-culture assay was conducted, and the cells were separated by a 0.4 μm pore size membrane to prevent direct cell–cell contact while allowing for the free exchange of EVs (Fig. 1H). WB analysis showed a significant increase in the level of Runx2 protein in VSMCs when co-cultured with ECs pre-treated with HG. However, the effect was reduced significantly when ECs were pre-treated with GW4869 (a widely utilized EVs release inhibitor) prior to co-culture with VSMCs (Fig. 1I), which indicating the critical role of EVs in promoting VSMC calcification. These results revealed that the EC^{HG}-EVs, rather than other factors, play a crucial role in promoting VSMC calcification in vitro.

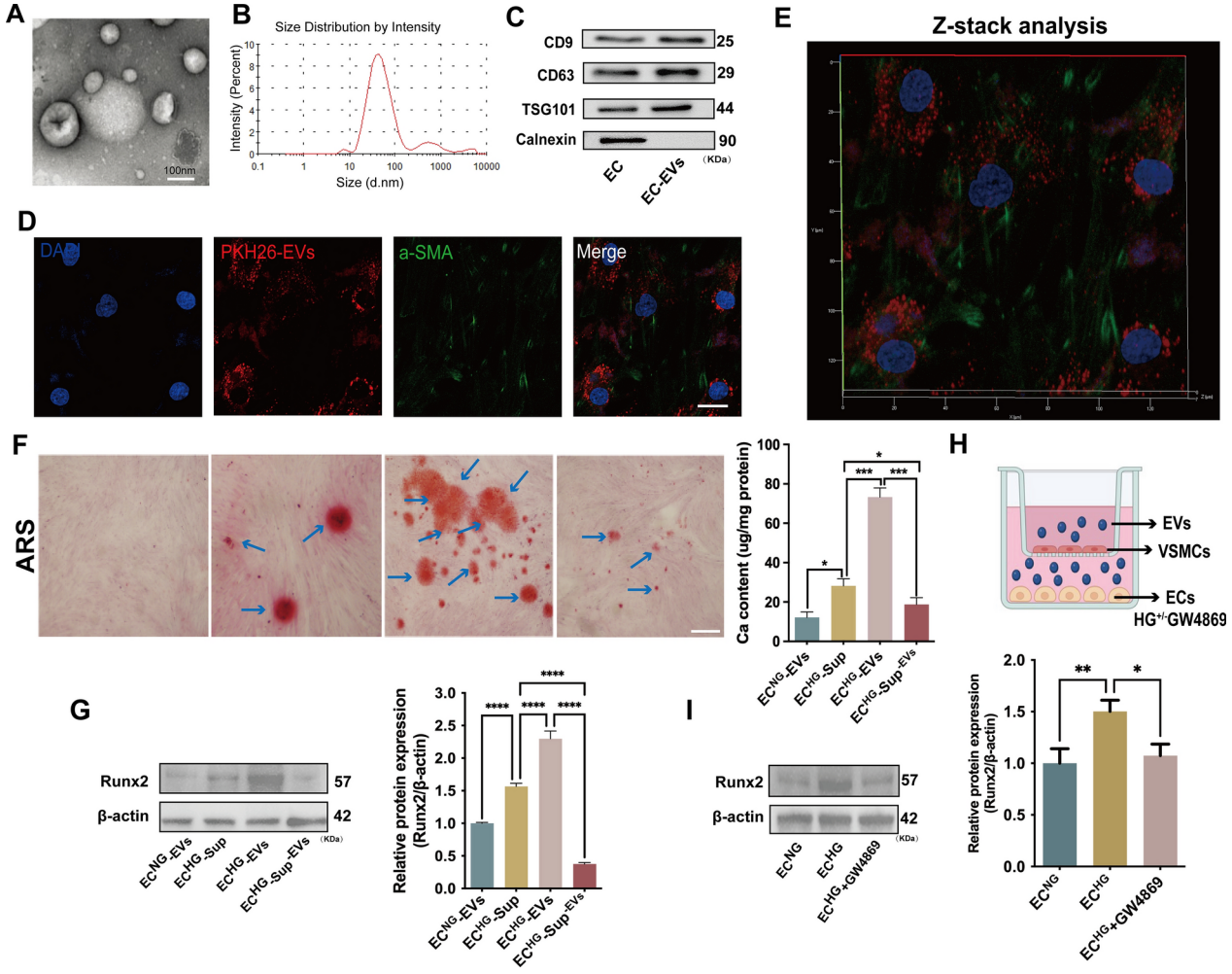

Fig. 1 EVs derived from HG-stimulated ECs exacerbated VSMC calcification. **A** Representative morphological analysis of EC-EVs by TEM (Scale bar = 100 nm). **B** Diameter distribution of EC-EVs by NTA; **C** the expression of CD9, CD63, TSG101 and Calnexin were detected by WB. **D**–**E** Laser scanning confocal microscope and Z-stack analysis showed that PKH26-labeled EC-EVs would be taken up by VSMCs and mainly located at the cytoplasm of VSMCs (PKH26 in red, DAPI in blue, and a-SMA in green) (scale bar = 20 μm). **F** ARS staining and quantification of the calcium content in VSMCs treated with EC^{NG}-EVs, EC^{HG}-Sup, EC^{HG}-EVs, EC^{HG}-Sup^{-EVs}, respectively. The blue arrows indicate mineralized nodules in VSMCs (Scale bar = 100 μm). **G** The expression of Runx2 protein was determined by WB in VSMCs incubated with EC^{NG}-EVs, EC^{HG}-Sup, EC^{HG}-EVs, EC^{HG}-Sup^{-EVs}, respectively. **H** ECs were pre-treated with HG and co-cultured with VSMCs in the trans-well units, either with or without the addition of GW4869; **I** the expression of Runx2 protein was measured by using WB. One-way ANOVA with Tukey's multiple comparisons test (**F**, **G**, **I**) was used. Three independent experiments were performed, and the representative data were shown. Data were shown as mean ± SD. ****$p < 0.0001$, ***$p < 0.001$, **$p < 0.005$, *$p < 0.05$. EVs, extracellular vesicles; TEM, transmission electron micrographs; NTA, nanoparticle tracking analysis; WB, western blot; EC^{NG}-EVs, EVs derived from normal-glucose induced ECs; EC^{HG}-EVs, EVs derived from high-glucose induced ECs; EC^{HG}-Sup, supernatant derived from high-glucose induced ECs; EC^{HG}-Sup^{-EVs}, supernatant derived from EC^{HG} with deprivation of EVs; ARS: alizarin red s

hsa_circ_0008362 was enriched in EC^{HG}-EVs and contributed to the exacerbation of VSMC calcification both in vitro and in vivo

Previous studies had demonstrated differential expression of multiple circRNAs in ECs under hyperglycemia [17, 18]. In addition, an RNA-sequencing approach detected the expression of different circRNAs in plasma EVs between normal and diabetic mice [19]. Through screening of microarray data reported in the above literatures and comprehensive analysis, only hsa_circ_0008362 and circ-Rnf169 were highly expressed in HG induced human ECs (supplemental Fig. 2A). However, previous studies had reported that circ-Rnf169 was involved in regulating cell proliferation and inhibiting epithelial-mesenchymal transition in diabetic nephropathy [20]. Considering the unclear role and mechanism of hsa_circ_0008362 in arterial calcification and it is highly conserved in human and mice, we chose hsa_circ_0008362 as the focus of the subsequent research. Firstly, the quantitative real-time polymerase chain reaction (qRT-PCR) results showed that hsa_circ_0008362 predominantly located in cytoplasm in EC^{HG} (Fig. 2A) as well as

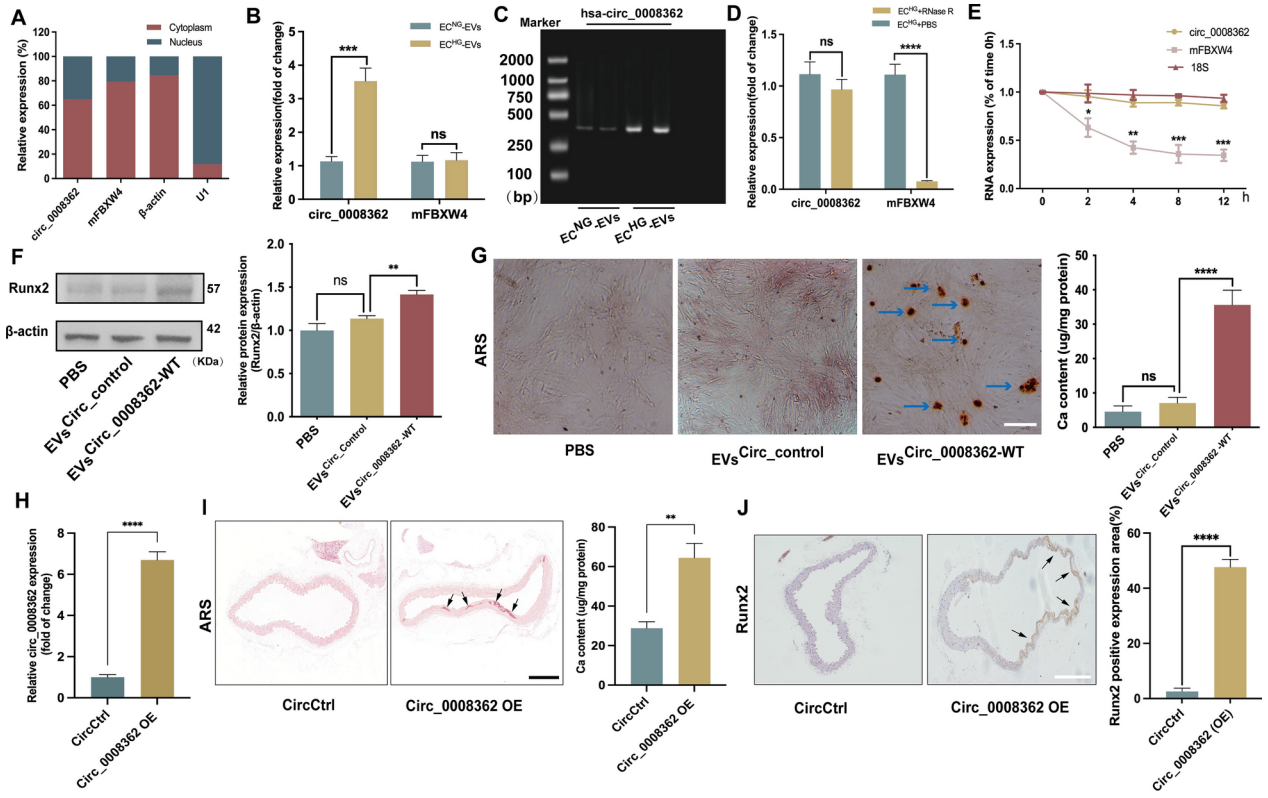

Fig. 2 hsa_circ_0008362 promoted VSMC calcification both in vitro and in vivo. **A** the location of hsa_circ_0008362 and mFBXW4 in EC^{HG} was demonstrated by qRT-PCR analysis. **B** qRT-PCR detected the different expression of circ_0008362 and mFBXW4 between EC^{NG}-EVs and EC^{HG}-EVs; **C** AGE detected the size of the PCR amplification product of hsa_circ_0008362 with double parallel experiment in EC^{NG}-EVs and EC^{HG}-EVs. **D** ECs was treated with RNase R and the expression of circ_0008362 and mFBXW4 were measured by qRT-PCR; **E** ECs was treated with 5 μg/ml actinomycin D (0, 2, 4, 8, 12 h) and the expression of circ_0008362 and mFBXW4 was detected by qRT-PCR; **F** the expression of Runx2 was measured by WB in VSMCs treated with $EVs^{Circ\_Control}$ or $EVs^{Circ\_0008362-WT}$, respectively. **G** ARS staining and quantification of the calcium content in VSMCs treated with $EVs^{Circ\_Control}$ or $EVs^{Circ\_0008362-WT}$. The blue arrows indicate mineralized nodules in VSMCs (scale bar = 100 μm). **H** qRT-PCR detected the expression of circ_0008362 in the aorta tissues of CircCtrl and Circ_0008362 OE mice. **I** ARS staining showed the arterial calcification in different mice (n = 5/group). The arrows indicate calcified arteries (scale bar = 200 μm). **J** Immunohistochemistry staining analysis of Runx2 expression in different mice. The arrows indicate the positive expression of Runx2 in the mice aorta (scale bar = 200 μm). One-way ANOVA with Tukey's multiple comparisons test (**B**, **D**, **F**, **G**) and Student's t-test (**E, H, I, J**) were used. Three independent experiments were performed, and representative data were shown. Data were shown as mean ± SD. $^{****}p < 0.0001$, $^{***}p < 0.001$, $^{**}p < 0.005$, $^{*}p < 0.05$. ns, no significance. WB, western blot; EC^{NG}-EVs, EVs derived from normal-glucose induced ECs; EC^{HG}-EVs, EVs derived from high-glucose induced ECs; $EVs^{Circ\_Control}$, EVs transfected with circular RNA negative control; $EVs^{Circ\_0008362-WT}$, EVs transfected with circ_0008362-wild type plasmid; CircCtrl, adeno-associated virus 9 negative control; Circ_0008362 OE, adeno-associated virus 9 circ_0008362 overexpression; AGE, agarose gel electrophoresis; ARS: alizarin red s

in EC^{NG} (supplemental Fig. 2B). Besides, the expression of hsa_circ_0008362 was increased significantly both in EC^{HG} and EC^{HG}-EVs, while its maternal gene FBXW4 (mFBXW4) expression was just increased in EC^{HG} but has no significant difference between EC^{NG}-EVs and EC^{HG}-EVs (Fig. 2B and supplemental Fig. 2C). Meanwhile, the agarose gel electrophoresis (AGE) verified that there indeed presence of circ_0008362 in EC^{HG}-EVs (Fig. 2C). Moreover, the RNase R and actinomycin D experiments were used to verify the ring structure and stability of hsa_circ_0008362 and demonstrated that hsa_circ_0008362 was more stable than mFBXW4, because it was almost not be digested by RNase R both in EC^{HG} and EC^{HG}-EVs, and it also not be degraded by 5 μg/ml of actinomycin D in EC^{HG} (Fig. 2D, E; supplemental Fig. 2D). These data verified that hsa_circ_0008362 has characteristics of circRNAs and highly expressed in EC^{HG}-EVs.

To explore the role of hsa_circ_0008362 in VSMC calcification, we first clarified that it was the EVs secreted by ECs carrying hsa_circ_0008362 to VSMCs rather than the VSMCs itself expresses hsa_circ_0008362, and AGE showed that the expression of hsa_circ_0008362 was increased significantly in VSMCs treated with EC^{HG}-EVs than EC^{NG}-EVs (supplemental Fig. 2E, F). Furthermore, qRT-PCR analysis showed the hsa_circ_0008362 expression was increased significantly in EVs transfected with circ_0008362 wild type plasmid ($EVs^{circ\_0008362-WT}$) compared to those transfected with the circular RNA negative control ($EVs^{circ\_Control}$) (supplemental Fig. 2G). As expected, a significant increase in Runx2 expression

and mineralized nodules formation in VSMCs transfected with EVs$^{circ_0008362-WT}$ (Fig. 2F, G). These results demonstrated that hsa_circ_0008362 enriched in EC^{HG}-EVs would be transmitted to VSMCs to promote VSMC calcification.

To demonstrate in vivo significance of circ_0008362 in vitro data, we built the recombinant adeno-associated virus 9 (AAV9) vectors carrying circ_0008362 or empty vector with a plasmid cytomegalovirus (pCMV) promoter (AAV9-pCMV-circ_0008362 or AAV9-pCMV-empty). AAV9-pCMV-empty served as negative control. Given that circ_0008362 was enriched in EC^{HG}-EVs and promoted VSMC calcification, we then overexpressed circ_0008362 using an AAV9 (circ_0008362 OE) that express circ_0008362 under the control of a cytomegalovirus promoter. Intravenous injection of circ_0008362 OE virus in mice was performed and AAV9 expressing empty (CircCtrl) were used as controls. qPCR showed that circ_0008362 OE increased the expression of circ_0008362 significantly (Fig. 2H). Accordingly, when injecting mice with circ_0008362 OE, the artery was calcified significantly when compared with CircCtrl injection mice (Fig. 2I). Meantime, the level of Runx2 in the aorta from the circ_0008362 OE treatment mice was much higher than that from the CircCtrl mice (Fig. 2J). Taken together, these results demonstrated that circ_0008362 would promote arterial calcification in vivo.

hsa_circ_0008362/ miR-1251-5p/Runx2 axial regulated VSMC calcification

We used Circular RNA Interactome and Circbank to predict the targets of hsa_circ_0008362 and found that three osteoblastic differentiation related miRNAs (miR-1251-5p, miR-217, miR-767-5p) were the potential targets of hsa_circ_0008362. However, qRT-PCR verified that only miR-1251-5p decreased significantly in VSMCs treated with EC^{HG}-EVs (supplemental Fig. 3A). Besides, there existed enough complementary sites between hsa_circ_0008362 and miR-1251-5p (Fig. 3A). Moreover, the expression of miR-1251-5p was opposite to hsa_circ_0008362 and decreased significantly in VSMCs with EC^{HG}-EVs treatment (supplemental Fig. 3A). Besides, RNA fluorescent in situ hybridization (FISH) showed that hsa_circ_0008362 and miR-1251-5p were co-localization in the cytoplasm of VSMCs (Fig. 3B), which indicating that hsa_circ_0008362 may potentially interact with miR-1251-5p.

In order to clarify the interaction between hsa_circ_0008362 and miR-1251-5p, gain- and loss-function was firstly used. When overexpression of hsa_circ_0008362 in VSMCs via transfecting circ_0008362 wild type (WT) plasmid, the expression of miR-1251-5p was significantly decreased when compared with Circ_Control (Fig. 3C). Meantime, the expression of hsa_circ_0008362 was decreased greatly when overexpression of miR-1251-5p, but increased significantly when inhibit the expression of miR-1251-5p (Fig. 3D). The effect of hsa_circ_0008362-WT plasmid and miR-1251-5p mimics or inhibitor were shown in the supplemental Fig. 3B and C, respectively. Moreover, biotin-labelled miR-1251-5p pull-down assay verified that the sequence of miR-1251-5p could highly bind with hsa_circ_0008362 (Fig. 3E). Additionally, RNA immunoprecipitation (RIP) assay showed that miR-1251-5p and hsa_circ_0008362 were substantially enriched by Ago2 antibody compared with control IgG antibody (Fig. 3F), which suggested that miR-1251-5p and hsa_circ_0008362 were present in RNA-induced silencing complex (RISC). These data suggested that hsa_circ_0008362 and miR-1251-5p could interact with each other in VSMCs.

MiRNAs usually exert their functions by interacting with the 3′untranslated region (3′UTR) or protein-coding sequence of target mRNAs. To search for the downstream mechanism of miR-1251-5p in regulating VSMC calcification, we used miRNADA, miRWalk and RNA22 to predict the possible targets of miR-1251-5p (supplemental Fig. 3D). Interestingly, the 3'UTR region of Runx2 was predicted to contain some potential binding sites for miR-1251-5p (Fig. 3A). WB showed the level of Runx2 protein was increased significantly in VSMCs treated with EC^{HG}-EVs (Fig. 3G). The following luciferase reporter assay demonstrated that enforced expression of miR-1251-5p markedly suppressed the luciferase activity of WT-Runx2 reporter, while no change was observed in the luciferase activity of Mut-Runx2 reporter (Fig. 3H). However, the expression of miR-1251-5p had no significant influence on the expression of Runx2 mRNA (supplemental Fig. 3E). Furthermore, qRT-PCR further showed that overexpression of hsa_circ_0008362 prominently increased Runx2 expression (Fig. 3I). These data indicated that Runx2 was the target of miR-1251-5p and hsa_circ_0008362 acted as a competing endogenous RNA (ceRNA) of miR-1251-5p to regulate the expression of Runx2 in VSMCs.

Finally, in order to explore whether hsa_circ_0008362 acted as a ceRNA of miR-1251-5p to regulate VSMC calcification depending on Runx2, we transfected VSMCs with small interfering RNA targeting Runx2 (siRunx2) to knock down its expression. The silencing efficiency assay revealed that siRunx2$^{2\#}$ exhibited the most potent effect in knocking down Runx2 expression (supplemental Fig. 3F), and it was selected for subsequent investigations. Accordingly, overexpression of miR-1251-5p significantly decreased the level of Runx2 protein as well as the mineral nodules formation, while inhibiting miR-1251-5p expression got the opposite results. However, knocking down the expression of Runx2, the effect of EC^{HG}-EVs and miR-1251-5p inhibitor in promoting

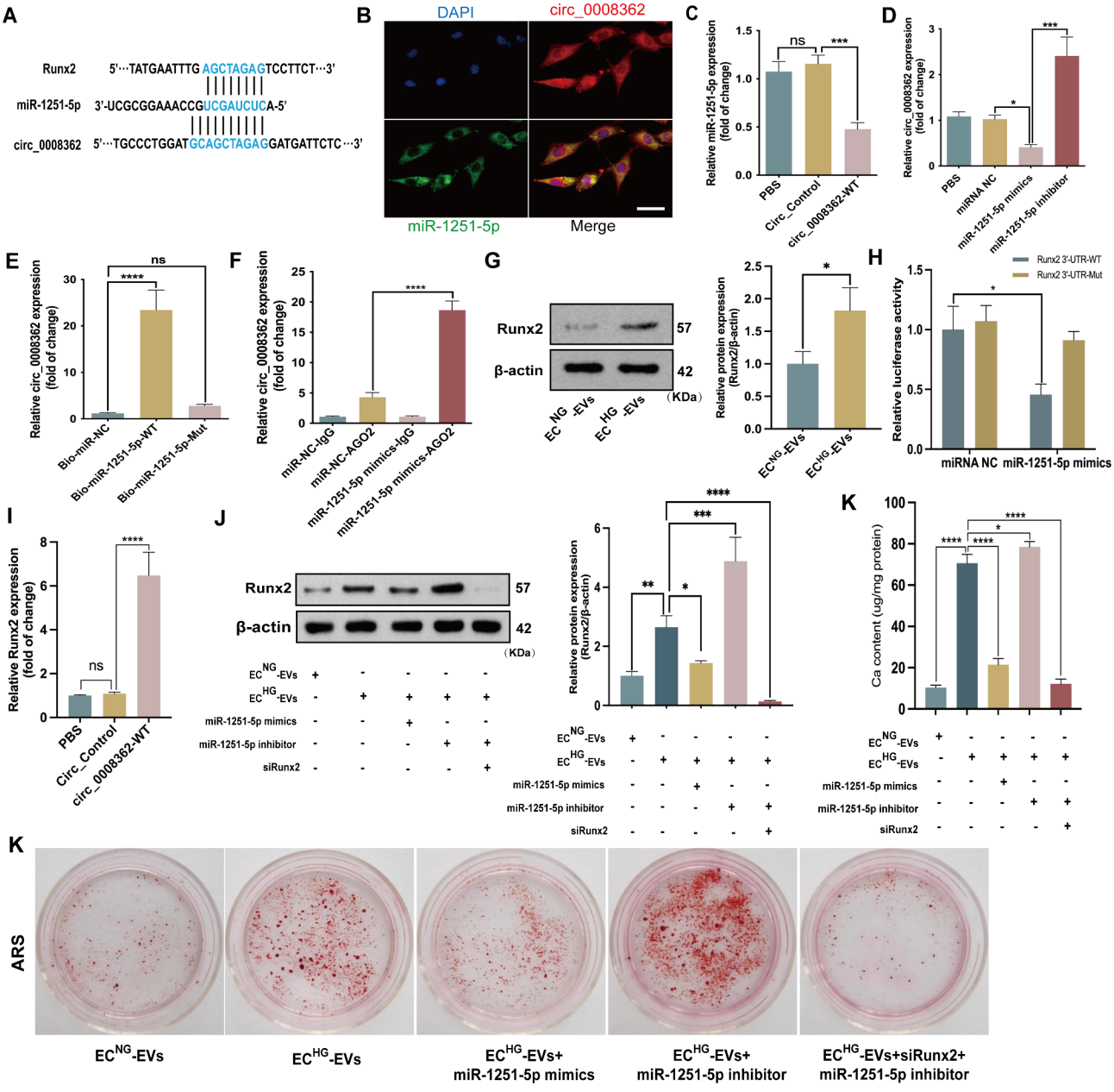

Fig. 3 hsa_circ_0008362/miR-1251-5p/Runx2 axial regulated VSMC calcification.**A** Schematic representation of putative target sites between miR-1251-5p and circ_0008362 as well as in Runx2 3′-UTR. **B** FISH showed the presence of circ_0008362 and miR-1251-5p in VSMCs. Scale bar = 50 μm. **C** the expression of miR-1251-5p in VSMCs transfected the vector of Circ_Control or Circ_0008362-WT. **D** the expression of hsa_circ_0008362 was detected by qPCR in VSMCs transfected by miR-1251-5p mimics or inhibitor. **E** The expression of circ_0008362 was detected by qRT-PCR after biotin-labeled miR-1251-5p pull-down assay. **F** RIP assay showed the binding efficiency of miR-1251-5p and circ_0008362 to Ago2 protein in VSMCs. **G** the expression of Runx2 was measured by WB in VSMCs treated with EC^{NG}-EVs or EC^{HG}-EVs. **H** Luciferase reporter assays showed the luciferase activities of Runx2 in VSMCs transfected with miR-1251-5p mimics or control oligos. **I** VSMCs were transfected with circ_0008362 plasmid and the level of Runx2 protein was measured by WB. **J** The level of Runx2 protein was measured by WB in VSMCs with different treatment. **K** ARS staining showed the mineralized nodules in VSMCs with different treatment, and the calcium content was quantified by spectrophotometry. One-way ANOVA with Tukey's multiple comparisons test (**C**, **D**, **E**, **F**, **H**, **I**, **J**, **K**) and the Student's test (G) were used. Three independent experiments were performed, and representative data were shown. Data were shown as mean ± SD. ****$p < 0.0001$, ***$p < 0.001$, **$p < 0.005$, *$p < 0.05$. ns: no significance. EC^{NG}-EVs, EVs derived from normal-glucose induced ECs; EC^{HG}-EVs, EVs derived from high-glucose induced ECs; Circ_Control, circular RNA negative control; circ_0008362-WT, circ_0008362-wild type plasmid; ARS, alizarin red s; RISC: RNA-induced silencing complex

VSMC calcification were almost abolished, which were evidenced by decreased level of Runx2 and mineralized nodules (Fig. 3J, K). These results demonstrated that hsa_circ_0008362/miR-1251-5p/Runx2 axial involved in regulating EC^{HG}-EVs induced VSMC calcification.

hsa_circ_0008362 interacts directly with Runx2 to promote VSMC calcification

Bioinformatics prediction and analysis showed that hsa_circ_0008362 has strong binding region with Runx2 protein (Fig. 4A) and suggested there exist direct binding sites between hsa_circ_0008362 and Runx2. Firstly, RNA pull-down assay demonstrated that Runx2 could highly bind biotin-labelled hsa_circ_0008362 in VSMCs

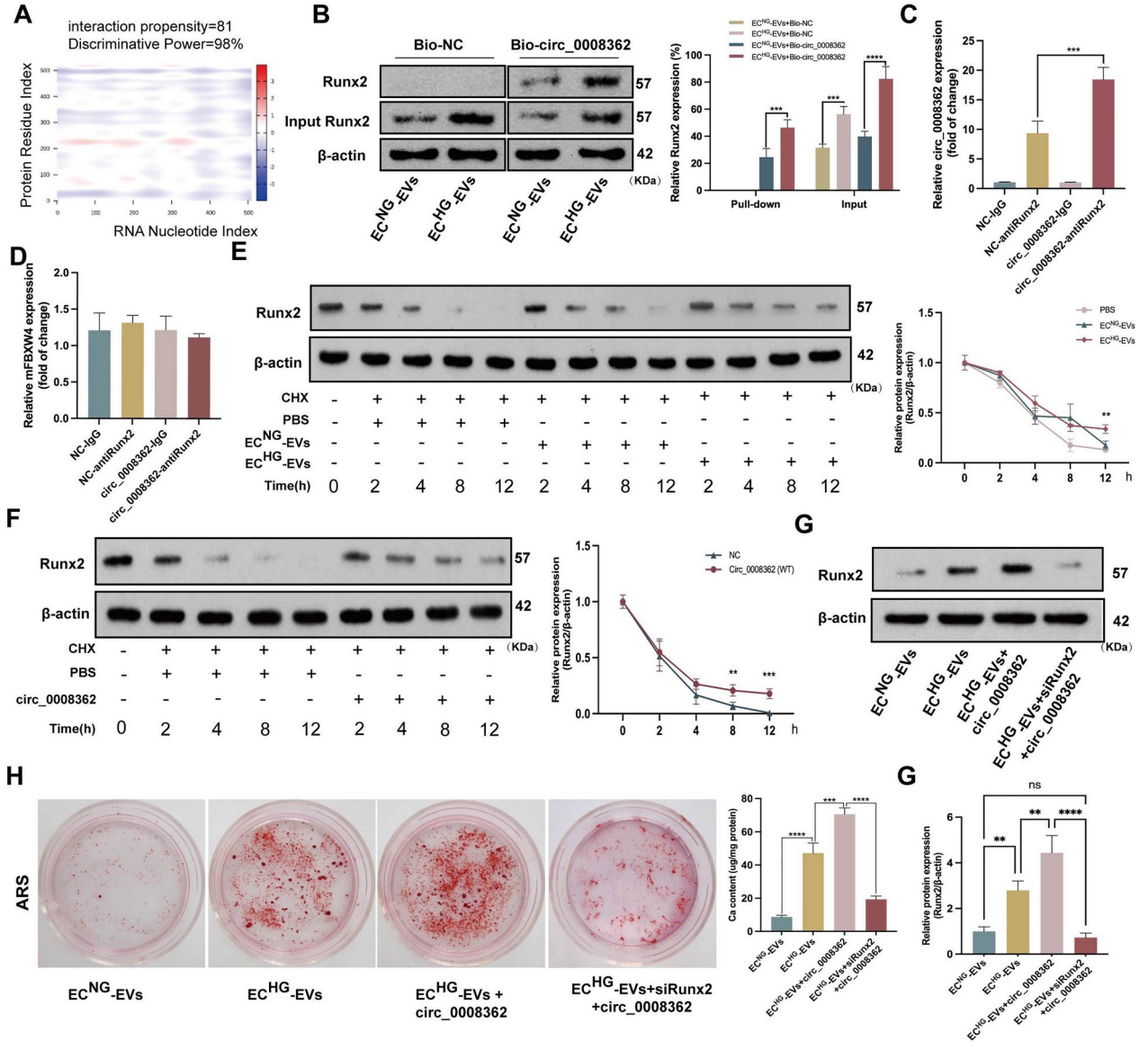

Fig. 4 hsa_circ_0008362 interacted directly with Runx2 to promote VSMC calcification. **A** hsa_circ_0008362 had strong binding region with Runx2 protein. **B** The expression of Runx2 was measured by WB after biotin-labelled circ_0008362 pull-down assay. **C**, **D** The expression of hsa_circ_0008362 and mFBXW4 detected by qRT-PCR in VSMCs via anti-Runx2 RIP experiments, respectively. **E** The half-life of Runx2 protein was measured by WB in VSMCs treated with EC^{NG}-EVs or EC^{HG}-EVs, accompanied with CHX (5ug/ml) treatment. **F** The degradation of Runx2 protein was measured by WB in VSMCs treated with hsa_circ_0008362 plasmid, accompanied with CHX (5 ug/ml) treatment. **G** The level of Runx2 protein was measured by WB in VSMCs with different treatment. **H** ARS staining showed the mineralized nodules in VSMCs with different treatment, and the calcium content was quantified by spectrophotometry. One-way ANOVA with Tukey's multiple comparisons test (**B**, **C**, **D**, **H**, **G**) was used. one-way ANOVA and Student's t-test (**E**, **F**) were used. Three independent experiments were performed, and representative data were shown. Data were shown as mean ± SD. $^{****}p < 0.0001$, $^{***}p < 0.001$, $^{**}p < 0.005$. ns, no significance; WB, western blot; EC^{NG}-EVs, EVs derived from normal-glucose induced ECs; EC^{HG}-EVs, EVs derived from high-glucose induced ECs; circ_0008362-WT, circ_0008362-wild type plasmid; ARS, alizarin red s; CHX, cycloheximide

with EC^{HG}-EVs treatment (Fig. 4B). Meanwhile, RIP experiments demonstrated that hsa_circ_0008362 could be bound with Runx2 (Fig. 4C), but there was no obvious interaction between mFBXW4 and Runx2 (Fig. 4D). In addition, Cycloheximide (CHX) experiment revealed that the half-life of Runx2 protein in VSMCs treated with EC^{HG}-EVs was longer compared with that treated with EC^{NG}-EVs (Fig. 4E). Moreover, overexpression of hsa_circ_0008362 would significantly slow the degradation of Runx2 protein (Fig. 4F). These data verified that hsa_circ_0008362 could direct interact with Runx2 and improve the stability of Runx2 protein.

To confirm whether hsa_circ_0008362 regulates VSMC calcification via direct interacted with Runx2, VSMCs was treated with hsa_circ_0008362 plasmid for overexpression of hsa_circ_0008362, accompanied with knocking down Runx2 expression via transfecting with siRunx2. The results demonstrated that overexpression of hsa_circ_0008362 exacerbated VSMC calcification induced by EC^{HG}-EVs, which was characterized by a significant increase of Runx2 expression and mineral nodules formation. However, the role of hsa_circ_0008362 of promoting VSMC calcification was almost abolished when knockdown of Runx2, as evidenced by decreased Runx2 expression and mineral nodule formation (Fig. 4G, H). Taken together, these results suggested that hsa_circ_0008362 promoted VSMC calcification dependent on direct interacting with Runx2 protein.

EC^{HG}-EVs mediated arterial calcification in diabetic mice

To further elucidate the function of EC^{HG}-EVs in vivo, firstly, we labelled EC^{HG}-EVs with the near-infrared dye DiR and administrated them to wild-type mice via tail vein injection. Photographs and organ imaging showed that there exhibited robust fluorescent signals of the DiR-labelled EC^{HG}-EVs in the aorta, heart, lung, kidney, liver and spleen within 12 h post-injection in mice (Fig. 5A–C). Furthermore, ARS staining showed that increased

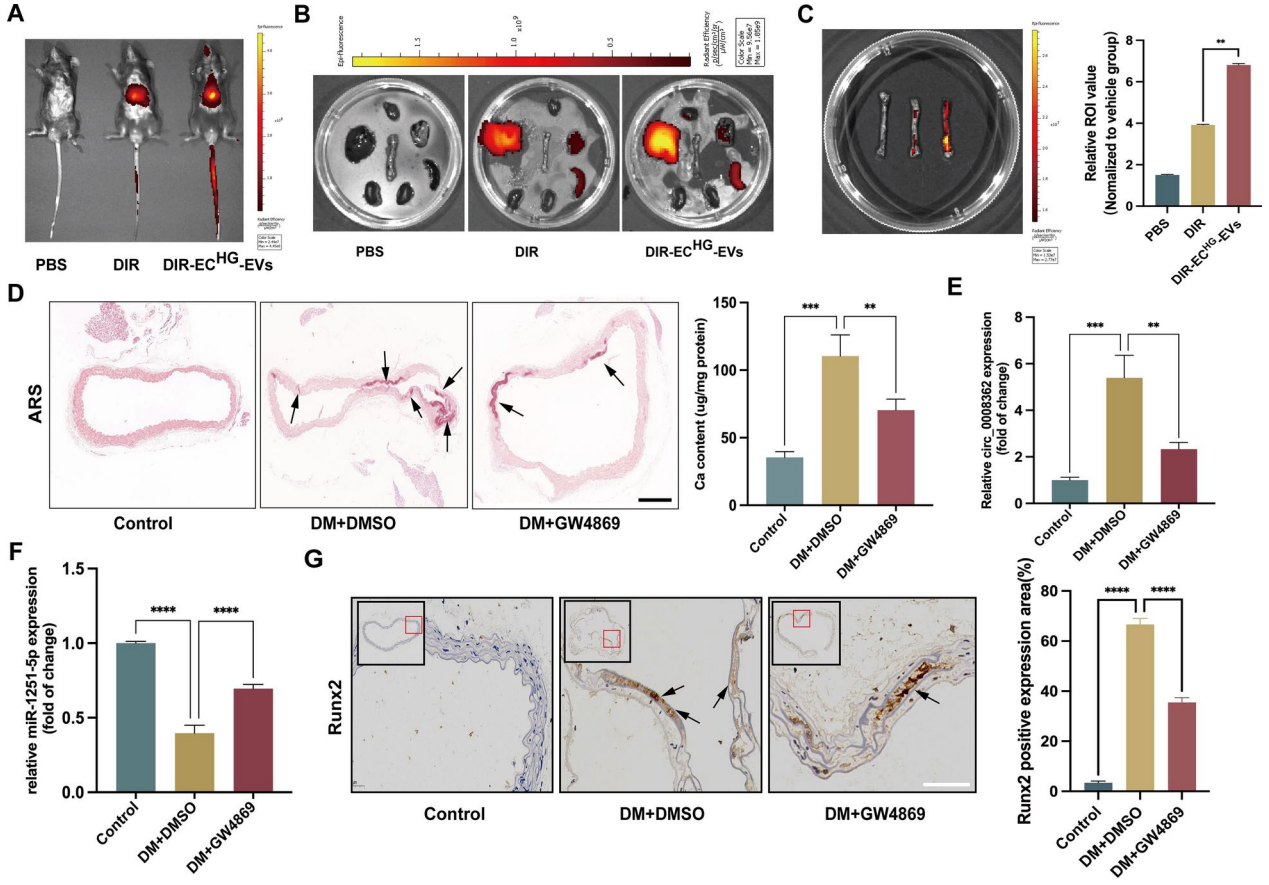

Fig. 5 EC^{HG}-EVs mediated arterial calcification in diabetic mice. **A**–**C** Fluorescence signals were detected in the living mice and organs (aorta, heart, lung, kidney, liver and spleen), respectively, after 12 h post-injection of DiR-labeled EC^{HG}-EVs in mice. **D** ARS staining analysis showed the arterial calcification in different mice (n = 5/group). The arrows indicate calcified arteries (scale bar = 200 μm). **E**–**F** The expression of circ_0008362 and miR-1251-5p in different mice arterial tissues (n = 5/group). **G** Immunohistochemistry staining analysis of Runx2 expression in different mice arterial tissues. The arrows indicate the positive expression of Runx2 in the mice aorta (scale bar = 50 μm). One-way ANOVA with Tukey's multiple comparisons test (**C**–**G**) was used. Three independent experiments were performed, and data were shown as mean ± SD. ****$p < 0.0001$, ***$p < 0.001$, **$p < 0.005$. EC^{HG}-EVs: EVs derived from high-glucose induced ECs; DM: diabetes mellitus; DMSO: Dimethyl sulfoxide; ARS: Alizarin red s

arterial calcification in diabetic mice compared with control mice. Interestingly, when injecting diabetic mice with GW4869, a pharmacological compound known to effectively inhibit EVs release in vivo, the effect of DM on promoting arterial calcification was partially blocked (Fig. 5D). In addition, qRT-PCR analysis revealed that the expression of circ_0008362 was increased significantly, while miR-1251-5p expression was significantly decreased in the arteries derived from diabetic mice comparison to that in the control group mice. However, when inhibiting the EVs release by GW4869, the expression of circ_0008362 was decreased, meantime miR-1251-5p expression was increased (Fig. 5E, F). Furthermore, our data demonstrated that the level of Runx2 in GW4869 pre-treatment mice was lower compared with that in diabetic mice showed by immunochemistry analysis (Fig. 5G). Taken together, it was truly the endogenous EVs that participate in regulating arterial calcification under hyperglycemia conditions. But the precise mechanism of circ_0008362 modulating arterial calcification requires further investigation.

Circulating hsa_circ_0008362 of plasma EVs was elevated in patients with DM and positively correlated with coronary and aortic calcification

Finally, in order to further verify the role of circulating hsa_circ_0008362 of plasma EVs in diabetic arterial calcification, the plasma EVs circulating hsa_circ_0008362 concentration, accompanied with coronary and aortic artery calcification scores in patients with DM were measured, as well as the age- and sex-matched normal control volunteers (supplemental Table 2). As shown in the computed tomography (CT) images, patients with DM had more serious coronary and aorta artery calcification, and both the coronary and aorta artery calcification scores (CACs and AACs) were significantly higher than normal controls (Fig. 6A–C). Meanwhile, hsa_circ_0008362 levels of plasma EVs were significantly higher in patients with DM as compared with those in matched normal controls (Fig. 6D). Furthermore, a positive correlation was identified between plasma EVs hsa_circ_0008362 and CACs as well as AACs in patients with DM (Fig. 6F–H). However, the level of plasma EVs hsa_circ_0008362 has no significant correlation with CACs or AACs in normal control participants (Fig. 6E–G). These data suggested that the increased hsa_circ_0008362 of plasma EVs was associated with arterial calcification in patients with DM.

Discussion

In the present study, we demonstrate that EVs derived from HG induced ECs promote VSMC calcification, and hsa_circ_0008362, enriched in EC^{HG}-EVs, mediates the pro-calcifying effect both in vitro and in vivo. Mechanistically, miR-1251-5p is verified to act as a downstream regulatory molecule of hsa_circ_0008362, and hsa_circ_0008362 could sponge with miR-1251-5p to promote VSMC calcification by upregulating the Runx2 of the miR-1251-5p target gene. Meanwhile, hsa_circ_0008362 would also directly interact with Runx2 to further enhance VSMC calcification. Additionally, we verify the role of both EC^{HG}-EVs and hsa_circ_0008362 in mice and analyze the correlation of hsa_circ_0008362 level of plasma EVs with CACs and AACs in patients with DM. Taken together, we demonstrate that hsa_circ_0008362/miR-1251-5p/Runx2 axial regulate VSMC calcification (Fig. 7). This study reveals a new insight to enhance our understanding of the molecular mechanism of VSMC calcification and provides a novel prevent and therapeutic approach for diabetic arterial calcification.

DM is a common and severe metabolic disease and it is associated with a greatly accelerated rate of macro- and micro-vascular complications, leading to renal failure, amputations, and cardiovascular events [21]. Medial arterial calcification, one of the important arterial complications in patients with DM, have been demonstrated to be an independent risk factor for cardiovascular diseases (CVD) [4]. The key process in medial arterial calcification is the trans-differentiation of VSMCs into osteoblast-like cells, resulting in an upregulation of ALP and Runx2 expression, along with the mineralized nodules formation [2, 22]. Previous studies had demonstrated that hyperglycemia is the main reason for arterial calcification in patients with DM [6, 23], but the mechanism remains unclear.

Arterial calcification is tightly associated with alterations in the structural and physiological functions of the vessel wall, mainly in ECs and VSMCs. It is well understood that hyperglycemia affects the function of ECs because the ECs are stimulated by various factors in the circulation of blood. Thereinto, Wang et al. reported that HG promoted HUVECs senescence by increasing the expression of the Krüppel-like factor 4 protein [16]. Besides, hyperglycemia could activate ECs to express adhesion proteins, E-selectin, intercellular adhesion molecule-1 and vascular cell adhesion molecule-1, and then initiate and accelerate atherosclerosis [24]. However, it is mainly the VSMC calcification of the medial artery in patients with DM and the mechanism how HG influence VSMC calcification is still unknown.

EVs, with a diameter ranging from 30 to 200 nm, are secreted by virtually all cell types and facilitate the transfer of biomolecules such as proteins, nucleic acids, and lipids from donor cells to recipient cells [25]. This natural intercellular transport mechanism plays a pivotal role in various aspects of human health and disease [26, 27]. For instance, colorectal cancer cells derived EVs caused ECs tipping to promote angiogenesis and tumor metastasis by activating Akt signaling pathway [27]. To the contrary,

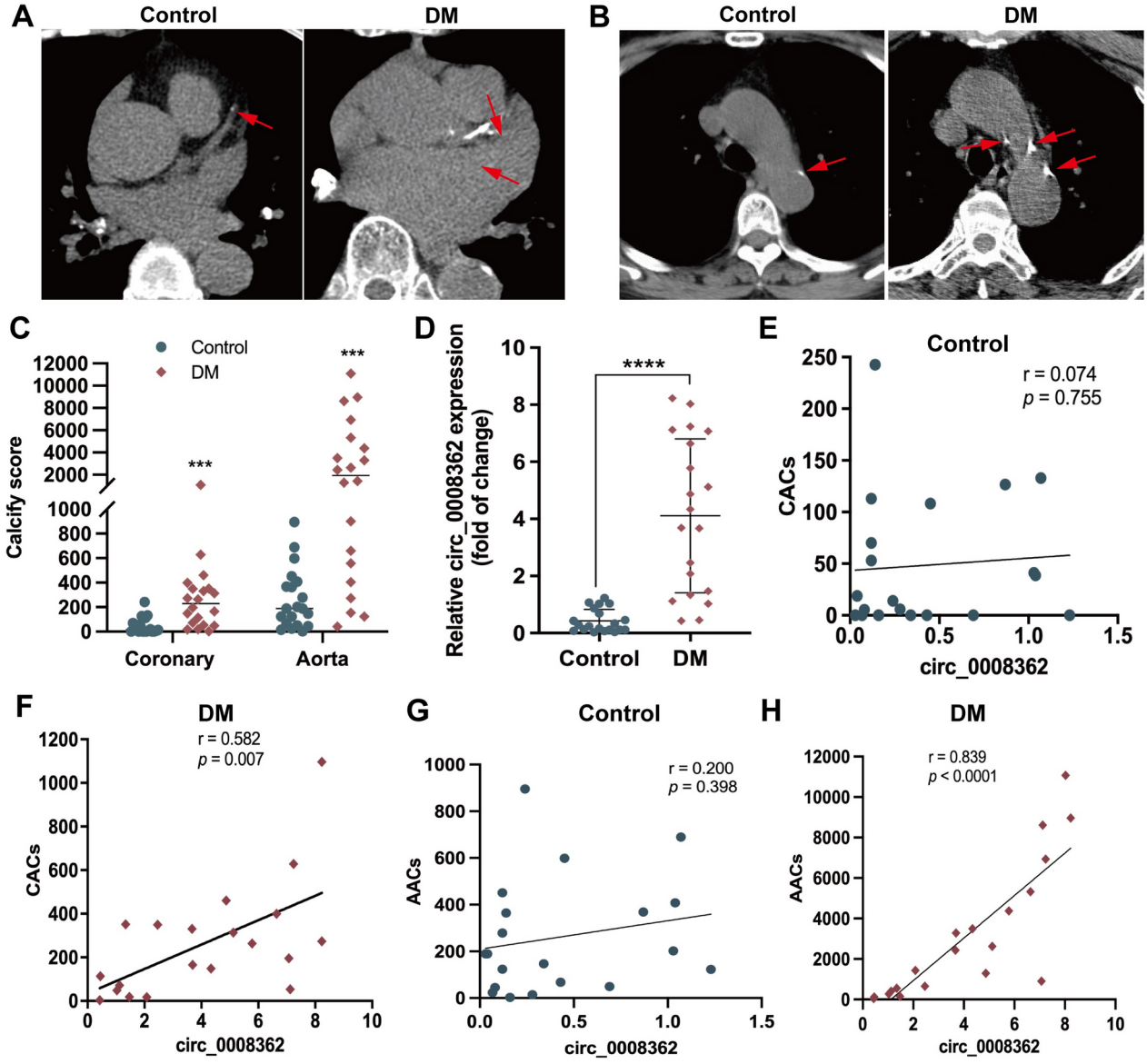

Fig. 6 Circulating plasma EVs hsa_circ_0008362 was correlated with arterial calcification in patients with DM. **A**–**C** CT images showed the coronary artery calcification as well as aorta artery calcification and quantified as CACs and AACs in normal control and DM group (n = 20). **D** The relative expression of hsa_circ_0008362 was detected by qRT-PCR in plasma EVs of normal control and patients with DM (n = 20). **E**–**H** Correlations between circ_0008362 of plasma EVs and CACs as well as AACs were analyzed using a Spearman's correlation analysis in normal control and patients with DM (n = 20). The normality of data distribution was assessed by Shapiro–Wilk test and Non-parametric Mann–Whitney U test for C and D. ****$p < 0.0001$, ***$p < 0.001$. ns, no significance; DM, diabetes mellitus; CACs, coronary artery calcification scores; AACs, aorta artery calcification scores

EC-derived EVs could also affect the function of other cells by transferring biological information to other cells [8, 10], including VSMCs [2]. Our previous study also had demonstrated that ECs induced by high concentration of inorganic phosphate would secrete EVs-derived miR-670-3p to promote VSMC calcification [2]. Besides, HG prompted ECs to secrete EVs containing various proteins which trigger the VSMC calcification and senescence [8, 28]. Accordingly, our present study re-affirms that EC^{HG}-EVs could be transferred to and internalized by VSMCs, thereby facilitating VSMC calcification. Furthermore, the organ-specific fluorescence signals observed in mice provide direct evidence supporting our findings that EC-derived EVs promote arterial calcification in diabetic mice. However, the specific mechanism by which EVs interact with target VSMCs needed further study.

CircRNAs, a novel class of endogenous ncRNA, characterized by its covalently closed continuous loop structure that lacks the 5′ or 3′ ends and presented tissue-specific and developmental stage-specific expression [29]. Numerous studies had reported a correlation between circRNAs and arterial calcification [30, 31]. Zhou et al.

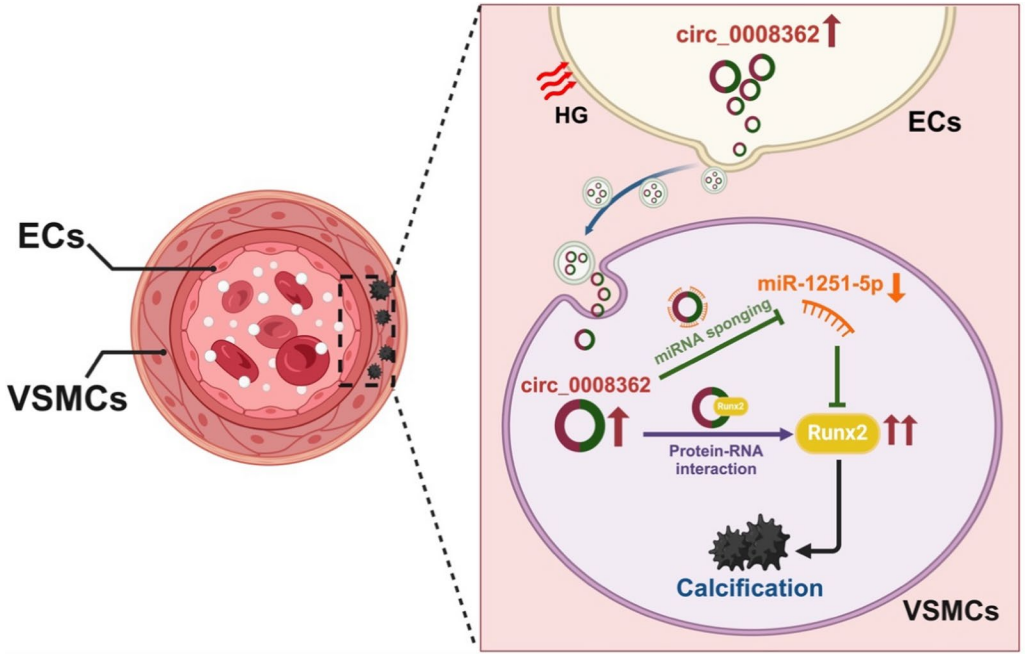

Fig. 7 Mechanism of hsa_circ_0008362 derived from EC-EVs regulating diabetic arterial calcification. Under hyperglycemia, ECs are stimulated by HG to release EVs and carry circ_0008362 to VSMCs. Circ_0008362, on the one hand, sponge with miR-1251-5p to promote VSMC calcification by upregulating the target gene-Runx2. On the other hand, circ_0008362 would also directly interact with Runx2 protein to increase the expression of Runx2, and then further enhance VSMC calcification. Finally, the accumulation of VSMC calcification resulted in arterial calcification in patients with DM. HG: high glucose; DM: diabetes mellitus. The figure created with BioRender.com

demonstrated that the expression of circSamd4a was decreased significantly in the calcified human aortic ECs and would be regarded as a biomarker for diagnosis of arterial calcification [31]. Another study verified that EV circRNA-0077930 from hyperglycaemia-stimulated ECs regulated VSMC senescence [16]. In our present study, we firstly hypothesis that ECs stimulated by HG would secrete EVs and that carry some circRNAs to modulate VSMC calcification. We search for the literatures and find the differential expression of multiple circRNAs in human ECs under hyperglycaemia [17–19] and selecte hsa_circ_0008362 for further study. Following a series of experiments, hsa_circ_0008362 derived from EC^{HG}-EVs would be taken up by VSMCs and promote VSMC calcification. Moreover, AAV9-mediated transfection of circ_0008362 could significantly increase circ_0008362 levels in the aorta at four weeks after AAV9 delivery compared with those in AAV9 CircCtrl treated groups, and in vivo Circ_0008362 OE specifically promote arterial calcification. This is the first time to demonstrate the role of hsa_circ_0008362 in arterial calcification.

CircRNAs usually exerting their functions through diverse molecular mechanisms, such as being miRNA sponges, regulating target gene transcription, participating in target gene splicing or translating genes into proteins [32]. "MiRNA sponge" is the most commonly reported mechanism of circRNAs involved in regulating gene expression [33]. Many RNA transcripts share binding sites with miRNAs, thus they compete with one another to act as ceRNAs to further regulate the pathogenesis and progression of numerous diseases [33, 34]. For example, circRNA CDR1 promoted pulmonary artery smooth muscle cell calcification by sponging miR-7-5p and then upregulating CAMK2D and CNN3 [34]. Similarly, another study demonstrated that hsa_circRNA_0008028 acted as a sponge of miR-182-5p to enhance VSMC proliferation, calcification, and autophagy by regulating TRIB3 in HG-induced VSMCs [35]. However, few investigations have elucidated the mechanism underlying of circRNAs in HG-induced ECs-derived EVs and its impact on VSMC calcification. Surprisingly, we find that there exist binding sites between hsa_circ_0008362 and miR-1251-5p. Besides, the gain- and loss-function, RNA pull down and RIP experiments verify that hsa_circ_0008362 could interact with miR-1251-5p.

It is known to us all that miRNAs typically exert their functions by modulating the translation or stability of target gene mRNA, thereby playing a pivotal role in the initiation and progression of arterial calcification [36, 37]. In the present study, gain- and loss-function and luciferase reporter assay confirm that Runx2 is the direct target of miR-1251-5p. Moreover, inhibiting the expression of miR-1251-5p, the expression of hsa_circ_0008362 as well as Runx2 are increased significantly and VSMC calcification is aggravated, which is verified by a significant

increase of mineralized nodules formation. Therefore, hsa_circ_0008362 acted as a sponge of miR-1251-5p by targeting Runx2 to regulate VSMC calcification. Actually, the roles of miR-1251-5p are just reported mainly in tumorigenesis and progression [38]. For instance, Shao et al. reported that miR-1251-5p could suppress TBCC and α/β tubulin expression in ovarian cancer cells, indicating its potential as a therapeutic target for ovarian cancer [38]. Knocking down of circ_0001666 resulted in upregulation of miR-1251 and downregulation of SOX4, thereby inhibiting epithelial-mesenchymal transition (EMT) in pancreatic cancer [39]. Thus, our study reveals a novel function of miR-1251-5p in the regulation of VSMC calcification. However, whether the effect and mechanism of hsa_circ_0008362/miR-1251-5p/Runx2 on arterial calcification in vivo need to be further studied.

CircRNAs also play a crucial role in regulating cell growth, differentiation, migration and apoptosis by serving as protein scaffolds that directly interact with various proteins [40–42]. For example, a recent study had shown that circFOXO3 could be bound to stress-related proteins FAK and HIF1α, as well as senescence related proteins ID-1 and E2F1 in the cytoplasm, preventing their nuclear entry and inhibiting their effects on cardiac fibroblasts aging and stress [42]. Huang et al. found that circNfix inhibited cardiomyocyte proliferation by enhancing the interaction between RBP Y box binding protein 1 and E3 ubiquitin ligase NEDD4-l in mouse cardiomyocytes [41]. Surprisingly, we further identify there exist directly binding sites between hsa_circ_0008362 and Runx2. Besides, functional experiments demonstrate that hsa_circ_0008362 would enhance the stability of Runx2 and significantly increase the expression of Runx2. Runx2 is the most important transcription factor for osteoblast differentiation [43, 44]. While silencing Runx2 expression, the effect of hsa_circ_0008362 promoting VSMC calcification has almost abolished and markedly alleviates VSMC calcification. In summary, upregulation of hsa_circ_0008362 directly regulates the expression of Runx2 through protein binding interaction, thereby exacerbating arterial calcification and providing a new perspective on the role of circ_0008362 in diabetic arterial calcification. Additionally, employing RNA pull-down assays combined with mass spectrometry [45] to identify novel much proteins interacting with circ_0008362 may offer crucial guidance for future research under pro-calcification condition.

Indeed, CAC [46] and AAC [47] are important forms of arterial calcification and could be increased in patients with DM. Both CACs and AACs detected by electron beam CT are often used to evaluate the severity of arterial calcification and they have significant prognostic value across a wild spectrum of risk factor profiles for cardiovascular events [48–50]. Previous studies had reported that patients with DM had higher CACs and AACs than those without DM [2, 50]. Additionally, CACs and AACs can predict mortality of cardiovascular diseases and provide additional prognostic information that obtained from clinical risk scores [51]. Therefore, it can be used as a predictor of risk stratification for cardiovascular events in patients with DM [50, 52, 53]. In this study, we observe a significantly higher CACs as well as AACs, and increased plasma hsa_circ_0008362 concentration has a positive correlation between CACs and AACs in patients with DM. However, there is no significant correlation between plasma hsa_circ_0008362 concentration and CACs or AACs in normal human. This may be due to almost lack of plasma EVs hsa_circ_0008362 in normal human, and ECs secrete enough hsa_circ_0008362 under the stimulation of hyperglycemia. These data suggest that plasma EVs hsa_circ_0008362 concentration may be used as a biomarker to evaluate arterial calcification in patients with DM, which suggests the potential development of a rapid assay kit for detecting hsa_circ_0008362 in plasma derived EVs, facilitating early diagnosis of arterial calcification progression in patients with DM. Recently, given engineered EVs have emerged as a novel and promising targeted drug delivery platform due to their natural origin, low toxicity, and exceptional biocompatibility [54–56], developing engineered EVs carried anti-hsa_circ_0008362 or overexpressed miR-1251-5p in the future might potentially delay arterial calcification progression and safeguard the cardiovascular system of patients with DM.

Conclusion

According to a series of comprehensive analysis, our present study identify and evaluate a novel circular RNA, hsa_circ_0008362, for the first time, and verify that it is enriched in the EVs derived from HG-induced ECs, and exacerbates VSMC calcification through a dual-mechanisms: hsa_circ_0008362 promotes VSMC calcification by competitively sponging with miR-1251-5p to promote Runx2 expression, as well as it directly interact with Runx2 protein to aggravate VSMC calcification. Therefore, gene therapy utilizing hsa_circ_0008362 presents a novel approach for the prevention and treatment of diabetic arterial calcification.

Materials and methods

Cell culture and transfection

Human umbilical vein endothelial cells (HUVECs) and human VSMCs were purchased from CHI Scientific, Inc. (7–1074) and Procell Technology Co. (CP-H081), respectively. FBS (Gibco, Invitrogen, New York, USA) was ultracentrifuged (Beckman, Germany) at 110,000×*g* for 90 min to eliminating exogenous EVs of FBS before culturing cells. HUVECs were cultured in F-12 k medium

(Hyclone), supplemented with 10% FBS, 0.05 mg/ml EC growth supplement (ECGS), 0.1 mg/ml heparin (Sciencell, San Diego, USA) and 1% penicillin/streptomycin. VSMCs were cultured in high glucose Dulbecco's Modified Eagle's Medium (DMEM, Hyclone, Logan, USA) supplemented with 10% FBS and 1% penicillin and streptomycin (P/S; Cat. No. 15070063, Gibco). Cells were maintained at 37 °C in a 95% humidified atmosphere with 5% CO_2 and passaged every 3–4 days.

For transient transfection of miR-1251-5p mimics, inhibitor or control oligos, hsa_circ_0008362 plasmid, as well as siRunx2 oligos using Lipofectamine 3000 (Invitrogen; Thermo Fisher Scientific, Inc., Waltham, MA, USA) according to the manufacturer's instructions as previous studies descripted. MiR-1251-5p mimics, inhibitor, and control oligos were purchased from Ribobio (Guangzhou, China). Hsa_circ_0008362 plasmid and siRunx2 were synthesized by GenePharma (Shanghai, China).

EVs isolation and identification

EVs were isolated from ECs induced with normal glucose (5 mmol/L, EC^{NG}-EVs) or high glucose (30 mmol/L, EC^{HG}-EVs) by ultracentrifugation (Beckman, Germany). Briefly, the cell culture supernatants were centrifuged at 300×*g* for 10 min, 2000×*g* for 30 min, 10,000×*g* for 30 min, and finally ultracentrifugation at 110,000×*g* for 90 min at 4 °C.

To isolate plasma EVs, the plasma sample was diluted with phosphate buffer saline (PBS) buffer in a ratio of 1:4 before ultracentrifugation. After ultracentrifugation at 110,000×*g* for 90 min at 4 °C, the EVs-enriched pellet was re-suspended in PBS and filtered through a 0.22 μm filter (Cat. No. SLGP033RS, Millipore) to remove residual cell debris. EVs were concentrated by 10 kDa centrifugal filter units (Millipore, Billerica, USA) until the final volume was about 100 μL. The protein quantification of EVs was performed using a BCA kit (Beyotime Biotechnology, Shanghai, China).

The concentration, distribution, and size of EVs were analyzed via nanoparticle tracking analysis (NTA) using a ZetaView PMX 110 (Particle Metrix, Germany) [57]. The morphology of EVs was identified using a Hitachi H-7650 transmission electron microscope (TEM; Hitachi, Tokyo, Japan). WB analysis was employed to detect EVs surface marker proteins, including CD9, CD63, TSG101, and Calnexin as previously described [2]. Besides, FBS marker BSA, as well as ECs markers, including CD31 and CD144 was measured by WB to further validate the purity and origin of EVs.

EVs uptake analysis

EVs were labelled with a PKH26 Red fluorescent cell linker kit (MINI26-1KT, Sigma) according to the manufacturer's instructions [2]. Briefly, 5μL of the PKH26 fluorescent probe was dissolved in 1 mL Diluent C solution and incubated with 100 μg EVs at room temperature (RT) for 5 min. 1 mL BSA was used to stop the staining reaction. The labelled EVs were precipitated by ultracentrifugation at 110,000×g for 90 min after washing with PBS. The labelled EVs were incubated with VSMCs at 37 °C for 12 h, and then VSMCs were fixed with 4% paraformaldehyde (PFA) for 30 min at RT and washed with PBS. And then VSMCs specific marker Alpha-smooth muscle actin (α-SMA) and DAPI (Invitrogen, Carlsbad, USA) were stained for 3 min and washed with PBS three times. The effects of EVs up-taken by VSMCs were observed under a laser scanning confocal microscope and Z-stack analysis (Zeiss LSM880, Germany).

In mice, the stock solution of DiR (D12731, Thermo Fisher Scientific) was prepared in ethanol and a 300 mmol/L working solution was prepared (Sigma-Aldrich). EC^{HG} -EVs were incubated with 2 mmol/L DiR for 30 min, and then washed with PBS and followed by 110,000×g for 90 min at 4 °C to remove free dye. The DiR dye alone or DiR-labelled EVs (100 μg per mice) were injected into wild-type (WT) mice via the tail vein, and 12 h later, the mice were imaged, and the thoracic aortas were collected. The aorta tissues were frozen in liquid nitrogen quickly to make frozen sections.

Transwell co-culture experiments

Six-well plates with a 0.4 μm pore-sized filter trans-well inserts (3412, Corning) were used following the manufacturer's instructions. ECs (1.5×10^5) cultured in the trans-well inserts and pre-treated with GW4869 (Sigma-Aldrich) for 48 h, and VSMCs (2×10^5) were cultured in the six-well plate. Before starting the co-culture experiments, both ECs and VSMCs were washed with PBS and then the trans-well insert ECs were put into the six-well plate with VSMCs. All co-culture experiments were done in complete DMEM supplement with HG (30 mM). After co-culture for 72 h, the protein of VSMCs were collected for further study.

ARS staining

ARS staining was performed as previously described [2]. Briefly, VSMCs were cultured with 100 μg/mL EC^{HG}-EVs for 14 days and fixed in 4% PFA for 30 min at RT and then stained with 1% (pH 4.2) ARS for 10 min at 37 °C. For artery samples, arteries were processed using the paraffin-embedded method, and the artery sections were stained with 1% (pH 4.2) ARS for about 1 min at RT. The stained matrixes were assessed and photographed with a digital microscope.

Alkaline phosphatase (ALP) staining

VSMCs were seeded in 24-well plates with different treatment for 7 days. After that VSMCs were washed with

PBS, fixed with 4% paraformaldehyde at RT for 30 min, and washed 3 times with PBS. Then VSMCs were incubated with ALP staining working solution (C3206, Beyotime Biotechnology, Shanghai, China) at RT for 30 min in the dark according to the manufacturer's instructions. After washing with PBS, the stained matrixes were assessed and photographed with a digital microscope.

RNA isolation and RNA analyses

Total RNA was extracted and purified from VSMCs using the miRNeasy® Mini Kit (Qiagen, cat. No. 217084) according to the standard protocol. Briefly, 700μL QIAzol lysis reagent was added, followed by chloroform extraction, and phase separation was achieved by centrifugation at 12,000×g for 15 min at 4 °C. Total RNA was isolated from the aqueous phase by spin column purification. Concentration and purity of RNA were assessed using the RNA Nano Drop 2000 System (Agilent Technologies, CA, USA).

Quantitative real-time polymerase chain reaction (qRT-PCR)

Total RNA was extracted from cultured ECs, VSMCs, and EC-EVs using the miRNeasy® Mini Kit (Qiagen, USA). The cDNA was synthesized from 1 μg of total RNA using RevertAid™ H Minus First Strand cDNA Synthesis Kit (Fermentas, Cat#: K1631) and qRT-PCR was carried out to analyze the RNA levels of hsa_circ_0008362 and Runx2. Briefly, 25 μl of reactants were incubated in a 96-well optical plate at 95 °C for 5 min, followed by 40 cycles of 95 °C for 20 s, 60 °C for 20 s and 72 °C for 20 s. For miR-1251-5p analysis, the All-in-One™-miRNA-qRT-PCR detection system was used (AOMD-Q060, Genecopoiea) as described by the manufacturer's protocol and using U6 snRNA as the reference. The detailed reaction conditions had been described in our previous study [2]. Briefly, a 25 μl reverse-transcription reaction was carried out for 60 min at 37 °C, 5 min at 85 °C, and a hold at 4 °C. The qRT-PCR was performed for 5 min at 95 °C, followed by 40 cycles of 10 s at 95 °C, 20 s at 60 °C, and 10 s at 72 °C. The relative mRNA and miRNA level were calculated using the relative standard curve method ($2^{-\triangle\triangle CT}$) and normalized to the relevant control value within the sample. The following PCR primers used in this study were purchased from Genecopoeia. Other gene sequence used in the study were shown in the Supplemental Table 1.

Identification of hsa_circ_0008362

Total RNA extracted from ECs or EC-EVs was digested with RNase R (Thermo Fisher Scientifc Inc, Waltham, MA, USA) for enrichment of circRNAs. Reverse transcription was conducted and the level of hsa_circ_0008362 and FBXW4 mRNA were detected by qRT-PCR. Besides, the size of the reverse transcription product (hsa_circ_0008362) was examined by 3% agarose gel electrophoresis (AGE). To determine the stability of hsa_circ_0008362, EC^{HG} treated with Actinomycin D (5 μg/ml) following the manufacturer's recommendation. The total RNA was collected and the level of hsa_circ_0008362 and FBXW4 mRNA were measured using qRT-PCR at 0, 2, 4, 8 and 12 h, respectively. For this measurement, 18 s RNA was used as the reference control because it is very stable and minimally affected by nucleases. The primers used in the study were shown in supplemental Table 1.

Fluorescent in situ hybridization (FISH)

FISH was performed to detect the location of hsa_circ_0008362 and miR-1251-5p using a RiboTM Fluorescent In Situ Hybridization Kit (Cat#: C10910, RiboBio Co., Ltd. Guangzhou, China). VSMCs were fixed with 4% paraformaldehyde for 30 min at RT and then incubated with 200 μl pre-hybridization buffer for 30 min at 37 °C. Hsa_circ_0008362 and miR-1251-5p FISH probe mix or 18 s or U6 was mixed with pre-hybridization buffer and then incubated with VSMCs at 37 °C overnight. The nuclei were stained with DAPI (Molecular Probe, Cat#: D1306). The results were observed under a Leica TCS SP5 laser confocal scanning microscope and analyzed using Image Pro Plus software (version 6.0).

Western blot (WB) analysis

Protein expression was determined by WB as previously described [6]. Briefly, 30 μg protein was analyzed by SDS gel electrophoresis and then transferred to a polyvinylidene fluoride membrane. After blocking with 5% nonfat milk, the membrane was incubated with primary antibodies, including anti-CD9 (20597-1-AP, 1: 2000, Proteintech), anti-CD63 (bs-23032R, 1:1000, BIOSS), anti-TSG101 (A1692, 1: 1000, abclonal), anti-calnexin (81938-1-RR, 1:5000, Proteintech), anti-CD31(A19014, 1: 2000, abclonal), anti-CD144 (AF6265, 1:1000, Affinity), anti-BSA (ab79827, 1:5000, Abcam), anti-BMP2 (66383-1-Ig, 1:2000, proteintech) and anti-Runx2 (ab23981, 1:1000, Abcam) at 4 °C overnight. The next day, the membranes were incubated with appropriate secondary antibody (1:4000 dilution) at RT for 1 h. The immunoreactive bands were processed using an enhanced chemiluminescence (ECL) kit (Cat#: RPN2232, Amersham Biosciences Ltd., UK) and then analyzed using Image-Pro Plus software (version 6.0).

RNA pull-down

RNA pull-down assays were carried out using a Pierce™ Magnetic RNA–Protein Pull-Down Kit (Cat#: 20164, Thermo Fisher Scientific). Briefly, for each assay, biotinylated miR-1251-5p or hsa_circ_0008362 was conjugated

to streptavidin magnetic beads. Then, the conjugated beads were incubated with the lysates from VSMCs in binding reaction buffer at 4 °C for 60 min with rotation. Next, the bound RNA–protein complexes were washed and eluted from the magnetic beads. Finally, RNAs in the complexes were purified and the enrichment patterns of hsa_circ_0008362 mRNA or Runx2 protein were measured using qRT-PCR and WB, respectively.

Luciferase reporter assay

Partial fragments of Runx2 3'UTR containing the predicted binding sites of miR-1251-5p were amplified by PCR and cloned into XbaI-FseI restriction sites of the pGL3 luciferase reporter vector (Promega, Madison, WI, USA). VSMCs were co-transfected with a luciferase reporter carrying Runx2 wild-type 3′ UTR, Runx2 mutant 3′ UTR, and miR-1251-5p mimics or scramble oligonucleotides. Then, 48 h after transfection, luciferase activities were quantified with the luciferase reporter assay system (Promega, USA) according to the protocols of the manufacturer. The nucleotide sequences of primers for the construction and mutation of 3′ UTR Runx2 mRNA were purchased from Ribobio (Guangzhou, China).

RNA immunoprecipitation (RIP) assay

RIP assay was performed using EZ-Magna RIP kit (No. 17-701, Millipore, Billerica, MA, USA) and Argonaute 2 (Ago2) antibody (Abcam, ab32381) to explore whether Runx2 and hsa_circRNA_0008362 existed in RNA-induced silencing complex (RISC). Briefly, VSMCs were lysed in RIP lysis buffer, followed by the incubation of protein A/G magnetic beads and antibody against rabbit IgG or Ago2. Then, RNAs in magnetic beads-binding complexes were purified. Lastly, qRT-PCR assay was employed to measure the enrichment patterns of hsa_circRNA_0008362 and FBXW4 mRNA by IgG or Ago2 antibody.

Cycloheximide (CHX) experiment

To examine whether the stability of Runx2 protein was affected by hsa_circ_0008362, VSMCs were pretreated with CHX (5ug/ml). Meanwhile, VSMCs was treated with EVs (EC^{NG}-EVs vs EC^{HG}-EVs) or hsa_circ_0008362 plasmid, the total protein were collected and the level of Runx2 protein was measured using WB at 0, 2, 4, 8 and 12 h, respectively.

Animals

The animal investigation conformed to published guidelines (National Research Council, The Care and Use of Laboratory Animals, 7th ed. Washington, DC: National Academies Press; 1996). All animal studies were formally approved by the Ethics Committee of the Second Xiangya Hospital, Central South University (Cat#: 2021161). 15 six to eight-week-old C57BL/6 mice were divided into three groups: control group, DM+DMSO group and DM+GW4869 group. DM mice model was established by streptozotocin (STZ, Sigma). Briefly, STZ (50 mg/kg) was freshly dissolved in 0.1 M phosphate-citrate buffer (pH 4.5) and injected into mice on five consecutive days. The control mice received the same dose of citrate buffer. Blood glucose levels were monitored after 3 days, and levels > 16.67 mM indicated the onset of DM [6]. The body weight and the level of blood glucose were taken before and every week after STZ injection. After 12 weeks, mice were sacrificed, and the thoracic aortas were dissected. The expression of circ_0008362 and miR-1251-5p were detected by qRT-PCR, the level of Runx2 protein was measured by WB and immunohistochemistry. ARS staining was used to detect artery calcification. Artery calcium content was measured by the o-cresolphthalein method. Total protein was quantified using the Bradford protein assay. All mice were housed with 12 h daylight/darkness in the animal house of the Second Xiangya Hospital.

In vivo circ_0008362 overexpression was achieved by AAV9 vectors. Recombinant AAV9 vectors carrying circ_0008362 or empty vector with a plasmid cytomegalovirus (pCMV) promoter (AAV9-pCMV-circ_0008362 or AAV9-pCMV-empty) were manufactured by JTS Scientific, (Wuhan, China). AAV9-pCMV-empty served as negative control. AAV9-pCMV-circ_0008362/empty vectors (5×10^{11} vector genomes/mice) were delivered by intravenous injection. Four weeks after AAV9 delivery, the overexpression of circ_0008362 was verified by qRT-PCR. The mice were sacrifice and the aorta were distracted after 12 weeks injection.

Immunohistochemistry analysis

The expression of Runx2 in the aorta tissues were examined by immunohistochemistry as described previously [22]. Briefly, sections of the arteries isolated from mice were fixed and processed using the paraffin-embedded method. Firstly, the artery tissue sections were baked at 65 °C for 2 h, followed by two rounds of dewaxing in xylene for 10 min and dehydrating in 99, 95 and 75% ethanol for 5 min each. Then, antigens were retrieved by trypsin solution and incubated with 3% hydrogen peroxide to clear endogenous peroxidase. After blocking with 5% BSA, sections were incubated with antibodies against Runx2 (ab23981, 1:100, Abcam) overnight at 4 °C. The next day, sections were incubated with a biotinylated secondary antibody and detected by the avidin–biotin-peroxidase complex and 3,3′-diaminobenzi dine chromogen (cat#: GK500710; Gene Tech, Shanghai). The immune-positive results were measured using a Nikon Eclipse microscope (Nikon Instruments Korea, Seoul, Korea) and analyzed using Image-Pro Plus software (version 6.0).

Clinical study

A total of 40 patients from the Second Xiangya Hospital of Central South University were enrolled in our study. The study included 20 patients with DM (DM group) and matched 20 normal controls (Control group). The study was approved by the Ethics Committee of the Second Xiangya Hospital of Central South University and conformed to the 1975 Declaration of Helsinki. Informed consents were gained from all subjects. The blood sample was collected in an EDTA tube. After centrifugation at 2000×*g* for 30 min at 4 °C, the plasma was aspirated and stored at−80 °C before use. The relative expression of hsa_circ_0008362 was measured by qRT-PCR. Additionally, the fasting venous blood samples of the patients were obtained after resting for at least 15 min. Lipid profile (TG, triglyceride; TC, total cholesterol; HDL-C, high-density lipoprotein cholesterol; LDL-C, low-density lipoprotein cholesterol) were collected and performed in the biochemistry laboratory at the Second Xiangya Hospital of Central South University.

The coronary computed tomography angiography (CCTA) and lung high resolution computed tomography coronary images were obtained from using the Siemens Somatom Definition computed tomography (CT) multilayer spiral scanner (Germany). Coronary artery calcification scores (CACs) and aorta artery calcification scores (AACs) were quantified via Agatston and analyzed by Siemens Ca Scoring software (syngo. via Siemens Healthcare GmbH). The CACs was calculated the sum of calcification scores of the calcified lesions from the four main branches of the coronary arteries: the left main, left anterior descending, left circumflex and right coronary artery. The AACs was calculated the sum of calcium scores of the calcific lesions from ascending aorta, aortic arch and descending aorta (thoracic aorta and part of abdominal aorta). The measure of the area of calcification times a fixed coeficient (the maximum pixel density decision) and the total score of the calcification of all faults were termed as the CACs and AACs.

Statistical analysis and reproducibility

The data analysis was performed with SPSS (version 27.0) and GraphPad Prism software (version 9.4.1). Quantitative variables were expressed as mean±standard deviation (SD), or median with minimum and maximum. Qualitative variables were expressed as numbers and percentages. The normality of data distribution was assessed by Shapiro–Wilk test before analysis, and a student's t-test was used to compare normally distributed data between two different groups. Comparisons of multiple groups were made using a one-way analysis of variance (ANOVA) with "Tukey's multiple comparisons test". The non-parametric Mann–Whitney U test was used to compare non-parametric datasets (non-normal distribution or n<6) between two groups. Categorical variables were compared using chi-squared tests. The correlations between plasma concentration of hsa_circ_0008362 and CACs or AACs were analyzed using a Spearman's correlation analysis. A level of $p<0.05$ was considered statistically significant. All experiments were repeated at least three times, with similar results. And representative experiment results were shown in the figures.

Abbreviations

3'UTR	3'Untranslated region
α-SMA	Alpha-smooth muscle actin
ALP	Alkaline phosphatas
AGE	Agarose gel electrophoresis
AACs	Aortic artery calcification scores
BSA	Bovine serum albumin
CACs	Coronary artery calcification scores
CeRNA	Competing endogenous RNA
CHX	Cycloheximide
CircRNAs	Circular RNAs
CT	Computed tomography
CircCtrl	Adeno-associated virus 9 negative control
Circ_0008362 OE	Adeno-associated virus 9 circ_0008362 overexpression
DM	Diabetes mellitus
DMEM	Dulbecco's modified eagle's medium
ECGS	Endothelial cell growth supplement
EC^{HG}-EVs	Extracellular vesicles derived from high glucose induced ECs
EC^{HG}-Sup^{-EVs}	Supernatant derived from high glucose induced ECs with deprivation of EVs
EC^{NG}-EVs	Extracellular vesicles from normal glucose induced ECs
ECs	Endothelial cells
EVs	Extracellular vesicles
$EVs^{circ\_control}$	EVs transfected with circular RNA negative control
$EVs^{circ\_0008362-WT}$	EVs transfected with circ_0008362 wild type plasmid
FBS	Foetal bovine serum
FISH	RNA fluorescent in situ hybridization
HUVECs	Human umbilical vein endothelial cells
miRNA	MicroRNA
NcRNAs	Noncoding RNAs
NTA	Nanoparticle tracking analysis
P/S	Penicillin and streptomycin
PBS	Phosphate buffer saline
PFA	Paraformaldehyde
Pre-mRNA	Pre-messenger RNAs
qRT-PCR	Quantitative real-time polymerase chain reaction
RIP	RNA immunoprecipitation
RISC	RNA-induced silencing complex
Runx2	Runt-related transcription factor 2
SiRunx2	Small interfering RNA targeting Runx2
TEM	Transmission electron microscopy
VSMCs	Vascular smooth muscle cells
WB	Western blot

Supplementary Information

The online version contains supplementary material available at https://doi.org/10.1186/s12933-024-02440-7 .

Supplementary Material 1

Acknowledgements

This work was supported by funding from the National Natural Science Foundation of China (Nos. 82100944, 82470927, 82100494, 82070910, and 82370892), Key R&D Plan of Hunan Province (2020SK2078), Clinical Research for Imaging in Human Province (2020SK4001), the Scientific Research Launch Project for new employees of the Second Xiangya Hospital of Central South University (No. 7600), the Health Research Project of Hunan Provincial Health

Commission (W20243019), the Fundamental Research Funds for the central Universities of Central South University (2024ZZTS0883)，National Clinical Key Specialties Major Research Projects (Z2023026) and the 2021 Research Project of Human Provincial Government commission (202103062278).

Author contributions
L-Q.Y and J.L are the corresponding authors and performed study design; X.L and S-Q.H performed the experiments, analyzed the data and wrote the manuscript; S-K.S, F.X, F-X-Z.L analyzed part of the data; X-B.L, F.W provided technical support; J-Y.D, M-H.Z, L-M.L, Y-Y.W, Y-L.W, K-X.T, R-R.C, B.H and J-J.Y revised the manuscript carefully; All authors read and approved the final paper.

Availability of data and materials
All relevant data and materials are available from the authors upon reasonable request.

Declarations

Ethics approval and consent to participate
The animal study was conducted in accordance with the guidelines outlined in the Care and Use of Laboratory Animals and received formal approval from the Ethical Review Board at the Second Xiangya Hospital of Central South University. All animals were housed in specific pathogen-free conditions, maintained on a 12/12-h dark–light cycle with a temperature of 22 °C and a humidity of 50–55%. The human study was approved by the Ethics Committee of the Second Xiangya Hospital of Central South University and conformed to the 1975 Declaration of Helsinki. Informed consents were gained from all subjects.

Consent for publication
All authors agree to be published.

Competing interests
The authors declare that they have no competing interests. Graphical abstract was created with biorender.com.

Author details
[1]Department of Radiology, The Second Xiangya Hospital, Central South University, Changsha 410011, Hunan, China
[2]National Clinical Research Center for Metabolic Diseases, Department of Metabolism and Endocrinology, The Second Xiangya Hospital, Central South University, 410011 Changsha, China
[3]Department of Pathology, The Second Xiangya Hospital, Central South University, 410011 Changsha, China
[4]Department of Radiology, The Second Affiliated Hospital of Xinjiang Medical University, Ürümqi 830054, China
[5]Department of Cardiovascular Surgery, The Second Xiangya Hospital, Central South University, Changsha 410011, China
[6]Clinical Research Center for Medical Imaging in Hunan Province, Department of Radiology Quality Control Center in Hunan Province, Changsha 410011, China

Received: 12 June 2024 / Accepted: 17 September 2024
Published online: 17 October 2024

References

1. Wu M, Rementer C, Giachelli CM. Vascular calcification: an update on mechanisms and challenges in treatment. Calcif Tissue Int. 2013;93(4):365–73.
2. Lin X, Shan SK, Xu F, Zhong JY, Wu F, Duan JY, Guo B, Li FX, Wang Y, Zheng MH, et al. The crosstalk between endothelial cells and vascular smooth muscle cells aggravates high phosphorus-induced arterial calcification. Cell Death Dis. 2022;13(7):650.
3. Chen A, Lan Z, Li L, Xie L, Liu X, Yang X, Wang S, Liang Q, Dong Q, Feng L, et al. SGLT2 inhibitor canagliflozin alleviates vascular calcification through suppression of NLRP3 inflammasome. Cardiovasc Res. 2023;119:2368.
4. Lanzer P, Hannan FM, Lanzer JD, Janzen J, Raggi P, Furniss D, Schuchardt M, Thakker R, Fok PW, Saez-Rodriguez J, et al. Medial arterial calcification: JACC state-of-the-art review. J Am Coll Cardiol. 2021;78(11):1145–65.
5. Demer LL, Tintut Y. Vascular calcification: pathobiology of a multifaceted disease. Circulation. 2008;117(22):2938–48.
6. Lin X, Xiang QY, Li S, Song WL, Wang YJ, Ni YQ, Zhao Y, Li C, Wang Y, Li HH, et al. BMF-AS1/BMF promotes diabetic vascular calcification and aging both in vitro and in vivo. Aging Dis. 2023;14(1):170–83.
7. Zoungas S, Chalmers J, Neal B, Billot L, Li Q, Hirakawa Y, Arima H, Monaghan H, Joshi R, Colagiuri S, et al. Follow-up of blood-pressure lowering and glucose control in type 2 diabetes. N Engl J Med. 2014;371(15):1392–406.
8. Lin X, Li S, Wang YJ, Wang Y, Zhong JY, He JY, Cui XJ, Zhan JK, Liu YS. Exosomal Notch3 from high glucose-stimulated endothelial cells regulates vascular smooth muscle cells calcification/aging. Life Sci. 2019;232: 116582.
9. Di Bella MA. Overview and update on extracellular vesicles: considerations on exosomes and their application in modern medicine. Biology (Basel). 2022;11(6):804.
10. Wu YY, Shan SK, Lin X, Xu F, Zhong JY, Wu F, Duan JY, Guo B, Li FX, Wang Y, et al. Cellular crosstalk in the vascular wall microenvironment: the role of exosomes in vascular calcification. Front Cardiovas Med. 2022;9: 912358.
11. Wang ZX, Luo ZW, Li FX, Cao J, Rao SS, Liu YW, Wang YY, Zhu GQ, Gong JS, Zou JT, et al. Aged bone matrix-derived extracellular vesicles as a messenger for calcification paradox. Nat Commun. 2022;13(1):1453.
12. Xu F, Zhong JY, Lin X, Shan SK, Bei G, Zheng MH, Wang Y, Li F, Cui RR, Wu F, et al. Melatonin alleviates vascular calcification and ageing through exosomal miR-204/miR-211 cluster in a paracrine manner. J Pineal Res. 2020;68:e12631.
13. Zheng MH, Shan SK, Lin X, Xu F, Wu F, Guo B, Li FX, Zhou ZA, Wang Y, Lei LM, et al. Vascular wall microenvironment: exosomes secreted by adventitial fibroblasts induced vascular calcification. J Nanobiotechnol. 2023;21(1):315.
14. Kristensen LS, Andersen MS, Stagsted LVW, Ebbesen KK, Hansen TB, Kjems J. The biogenesis, biology and characterization of circular RNAs. Nat Rev Genet. 2019;20(11):675–91.
15. Wu J, Qi X, Liu L, Hu X, Liu J, Yang J, Yang J, Lu L, Zhang Z, Ma S, et al. Emerging epigenetic regulation of circular RNAs in human cancer. Mol Ther Nucleic Acids. 2019;16:589–96.
16. Wang S, Zhan J, Lin X, Wang Y, Wang Y, Liu Y. CircRNA-0077930 from hyperglycaemia-stimulated vascular endothelial cell exosomes regulates senescence in vascular smooth muscle cells. Cell Biochem Funct. 2020;38(8):1056–68.
17. Jin G, Wang Q, Hu X, Li X, Pei X, Xu E, Li M. Profiling and functional analysis of differentially expressed circular RNAs in high glucose-induced human umbilical vein endothelial cells. FEBS Open Bio. 2019;9(9):1640–51.
18. Shang FF, Luo S, Liang X, Xia Y. Alterations of circular RNAs in hyperglycemic human endothelial cells. Biochem Biophys Res Commun. 2018;499(3):551–5.
19. Shou Y, Hu L, Zhang W, Gao Y, Xu P, Zhang B. Determination of electroacupuncture effects on circRNAs in plasma exosomes in diabetic mice: an RNA-sequencing approach. Evid Based Complement Alternat Med. 2019;2019:7543049.
20. Ling L, Tan Z, Zhang C, Gui S, Cui Y, Hu Y, Chen L. CircRNAs in exosomes from high glucose-treated glomerular endothelial cells activate mesangial cells. Am J Transl Res. 2019;11(8):4667–82.
21. Nathan DM, Lachin JM, Bebu I, Burch HB, Buse JB, Cherrington AL, Fortmann SP, Green JB, Kahn SE, Kirkman MS, et al. Glycemia reduction in type 2 diabetes—microvascular and cardiovascular outcomes. N Engl J Med. 2022;387(12):1075–88.
22. Li FX, Liu JJ, Xu F, Shan SK, Zheng MH, Lei LM, Lin X, Guo B, Li CC, Wu F, et al. Cold exposure protects against medial arterial calcification development via autophagy. J Nanobiotechnol. 2023;21(1):226.
23. Rogers MA, Aikawa E. Modifying vascular calcification in diabetes mellitus: contribution of O-GlcNAcylation. Circ Res. 2014;114(7):1074–6.
24. Mastrogiacomo L, Ballagh R, Venegas-Pino DE, Kaur H, Shi P, Werstuck GH. The effects of hyperglycemia on early endothelial activation and the initiation of atherosclerosis. Am J Pathol. 2023;193(1):121–33.
25. Arya SB, Collie SP, Parent CA. The ins-and-outs of exosome biogenesis, secretion, and internalization. Trends Cell Biol. 2023;90:108.
26. Nikdoust F, Pazoki M, Mohammadtaghizadeh M, Aghaali MK, Amrovani M. Exosomes: potential player in endothelial dysfunction in cardiovascular disease. Cardiovasc Toxicol. 2022;22(3):225–35.
27. Chen C, Liu Y, Liu L, Si C, Xu Y, Wu X, Wang C, Sun Z, Kang Q. Exosomal circTUBGCP4 promotes vascular endothelial cell tipping and colorectal cancer metastasis by activating Akt signaling pathway. J Exp Clin Cancer Res. 2023;42(1):46.
28. Li S, Zhan JK, Wang YJ, Lin X, Zhong JY, Wang Y, Tan P, He JY, Cui XJ, Chen YY, et al. Exosomes from hyperglycemia-stimulated vascular endothelial cells contain versican that regulate calcification/senescence in vascular smooth muscle cells. Cell Biosci. 2019;9:1.

29. Ju J, Song YN, Chen XZ, Wang T, Liu CY, Wang K. circRNA is a potential target for cardiovascular diseases treatment. Mol Cell Biochem. 2022;477(2):417–30.
30. Ryu J, Kwon DH, Choe N, Shin S, Jeong G, Lim YH, Kim J, Park WJ, Kook H, Kim YK. Characterization of circular RNAs in vascular smooth muscle cells with vascular calcification. Mol Ther Nucleic Acids. 2020;19:31–41.
31. Zhou Y, Liu Y, Xuan S, Jin T, Chen K, Wu Z, Su W, Chen L, Zong G. CircSamd4: a novel biomarker for predicting vascular calcification. J Clin Lab Anal. 2022;36(1): e24156.
32. Zang J, Lu D, Xu A. The interaction of circRNAs and RNA binding proteins: an important part of circRNA maintenance and function. J Neurosci Res. 2020;98(1):87–97.
33. Ikeda Y, Morikawa S, Nakashima M, Yoshikawa S, Taniguchi K, Sawamura H, Suga N, Tsuji A, Matsuda S. CircRNAs and RNA-binding proteins involved in the pathogenesis of cancers or central nervous system disorders. Noncoding RNA. 2023;9(2):23.
34. Ma C, Gu R, Wang X, He S, Bai J, Zhang L, Zhang J, Li Q, Qu L, Xin W, et al. circRNA CDR1as promotes pulmonary artery smooth muscle cell calcification by upregulating CAMK2D and CNN3 via sponging miR-7-5p. Mol Ther Nucleic Acids. 2020;22:530–41.
35. Shi L, Li Y, Shi M, Li X, Li G, Cen J, Liu D, Wei C, Lin Y. Hsa_circRNA_0008028 deficiency ameliorates high glucose-induced proliferation, calcification, and autophagy of vascular smooth muscle cells via miR-182-5p/TRIB3 Axis. Oxid Med Cell Longev. 2022;2022:5142381.
36. Lin X, Xu F, Cui RR, Xiong D, Zhong JY, Zhu T, Li F, Wu F, Xie XB, Mao MZ, et al. Arterial calcification is regulated via an miR-204/DNMT3a regulatory circuit both in vitro and in female mice. Endocrinology. 2018;159(8):2905–16.
37. Lin X, Zhan JK, Zhong JY, Wang YJ, Wang Y, Li S, He JY, Tan P, Chen YY, Liu XB, et al. lncRNA-ES3/miR-34c-5p/BMF axis is involved in regulating high-glucose-induced calcification/senescence of VSMCs. Aging (Albany NY). 2019;11(2):523–35.
38. Shao Y, Liu X, Meng J, Zhang X, Ma Z, Yang G. MicroRNA-1251-5p promotes carcinogenesis and autophagy via targeting the tumor suppressor TBCC in ovarian cancer cells. Mol Ther. 2019;27(9):1653–64.
39. Zhang R, Zhu W, Ma C, Ai K. Silencing of circRNA circ_0001666 represses EMT in pancreatic cancer through upregulating miR-1251 and downregulating SOX4. Front Mol Biosci. 2021;8: 684866.
40. Chen LL. The expanding regulatory mechanisms and cellular functions of circular RNAs. Nat Rev Mol Cell Biol. 2020;21(8):475–90.
41. Huang S, Li X, Zheng H, Si X, Li B, Wei G, Li C, Chen Y, Chen Y, Liao W, et al. Loss of super-enhancer-regulated circRNA Nfix induces cardiac regeneration after myocardial infarction in adult mice. Circulation. 2019;139(25):2857–76.
42. Du WW, Yang W, Chen Y, Wu ZK, Foster FS, Yang Z, Li X, Yang BB. Foxo3 circular RNA promotes cardiac senescence by modulating multiple factors associated with stress and senescence responses. Eur Heart J. 2017;38(18):1402–12.
43. Qin X, Jiang Q, Komori H, Sakane C, Fukuyama R, Matsuo Y, Ito K, Miyazaki T, Komori T. Runt-related transcription factor-2 (Runx2) is required for bone matrix protein gene expression in committed osteoblasts in mice. J Bone Miner Res. 2021;36(10):2081–95.
44. Cui RR, Li SJ, Liu LJ, Yi L, Liang QH, Zhu X, Liu GY, Liu Y, Wu SS, Liao XB, et al. MicroRNA-204 regulates vascular smooth muscle cell calcification in vitro and in vivo. Cardiovasc Res. 2012;96(2):320–9.
45. Hui Y, Wenguang Y, Wei S, Haoran W, Shanglei N, Ju L. circSLC4A7 accelerates stemness and progression of gastric cancer by interacting with HSP90 to activate NOTCH1 signaling pathway. Cell Death Dis. 2023;14(7):452.
46. Liabeuf S, Bourron O, Olivier B, Vemeer C, Theuwissen E, Magdeleyns E, Aubert CE, Brazier M, Mentaverri R, Hartemann A, Massy ZA. Vascular calcification in patients with type 2 diabetes: the involvement of matrix Gla protein. Cardiovasc Diabetol. 2014;13:85.
47. Wu Z, Yu S, Zhang H, Guo Z, Zheng Y, Xu Z, Li Z, Liu X, Li X, Chen S, et al. Combined evaluation of arterial stiffness, glycemic control and hypertension for macrovascular complications in type 2 diabetes. Cardiovasc Diabetol. 2022;21(1):262.
48. Agatston AS, Janowitz WR, Hildner FJ, Zusmer NR, Viamonte M Jr, Detrano R. Quantification of coronary artery calcium using ultrafast computed tomography. J Am Coll Cardiol. 1990;15(4):827–32.
49. Agarwal S, Cox AJ, Herrington DM, Jorgensen NW, Xu J, Freedman BI, Carr JJ, Bowden DW. Coronary calcium score predicts cardiovascular mortality in diabetes: diabetes heart study. Diabetes Care. 2013;36(4):972–7.
50. Churchill TW, Rasania SP, Rafeek H, Mulvey CK, Terembula K, Ferrari V, Jha S, Lilly SM, Eraso LH, Reilly MP, Qasim AN. Ascending and descending thoracic aorta calcification in type 2 diabetes mellitus. J Cardiovasc Comput Tomogr. 2015;9(5):373–81.
51. Reaven PD, Sacks J. Coronary artery and abdominal aortic calcification are associated with cardiovascular disease in type 2 diabetes. Diabetologia. 2005;48(2):379–85.
52. Nassar M, Nso N, Emmanuel K, Alshamam M, Munira MS, Misra A. Coronary artery calcium score directed risk stratification of patients with type-2 diabetes mellitus. Diabetes Metab Syndr. 2022;16(6): 102503.
53. Ferket BS, Hunink MGM, Masharani U, Max W, Yeboah J, Burke GL, Fleischmann KE. Lifetime cardiovascular disease risk by coronary artery calcium score in individuals with and without diabetes: an analysis from the multi-ethnic study of atherosclerosis. Diabetes Care. 2022;45(4):975–82.
54. Tian J, Han Z, Song D, Peng Y, Xiong M, Chen Z, Duan S, Zhang L. Engineered exosome for drug delivery: recent development and clinical applications. Int J Nanomed. 2023;18:7923–40.
55. Mondal J, Pillarisetti S, Junnuthula V, Saha M, Hwang SR, Park IK, Lee YK. Hybrid exosomes, exosome-like nanovesicles and engineered exosomes for therapeutic applications. J Control Release. 2023;353:1127–49.
56. Östgren CJ, Otten J, Festin K, Angerås O, Bergström G, Cederlund K, Engström G, Eriksson MJ, Eriksson M, Fall T, et al. Prevalence of atherosclerosis in individuals with prediabetes and diabetes compared to normoglycaemic individuals-a Swedish population-based study. Cardiovasc Diabetol. 2023;22(1):261.
57. Yekula A, Minciacchi VR, Morello M, Shao H, Park Y, Zhang X, Muralidharan K, Freeman MR, Weissleder R, Lee H, et al. Large and small extracellular vesicles released by glioma cells in vitro and in vivo. J Extracell Vesicles. 2020;9(1):1689784.

Publisher's Note